General comments:

In this paper, Chan et al. presented the long-term MAX-DOAS measurements of NO2 and HCHO profiles in Nanjing. The data are used to validate OMI NO2 and HCHO products, discuss the effects of a-priori profiles on OMI retrievals, analyze effects of regional transports, and effects of pollution control measures during the Youth Olympic Games. In general the scientific topic is meaningful, and the MAX-DOAS data quality is well proved. However the authors need to give more deep discussions in many parts to firmly prove the conclusions. Generally I have three major concerns below:

1) Regarding the comparisons with the OMI data in section 3.2, the authors should also show the comparisons of a-priori profile shapes of OMI NO2 retrievals with the NO2 profiles measured by MAX-DOAS for the discussion on the effect of a-priori profiles. In addition, the authors also need to discuss the a-priori effect for HCHO even in the case that a good agreement is found. It is very important to see if good agreements of HCHO profile shapes can been also seen between MAX-DOAS and OMI a-priori.

The underestimation of OMI NO2 VCDs is up to 50% compared to MAX-DOAS data shown in Fig. 2. However the previous study in Wuxi, see Wang et al. 2017, shows the underestimation is ~20%. One major difference is that the NO2 product is from NASA in your study, but from DOMINO v2 in Wang et al., 2017. Are there big differences of both OMI NO2 data sets? Why are there big differences? In order to answer the questions, the author needs to do comparisons also with the DOMINO v2 product. Meanwhile DOMINO v2 is an official product which is well known and widely used. In addition the author demonstrates that "Measurements with such large spatial coverage are probably difficult to capture the spatial gradient of NO2 and resulted in an underestimation over pollution hot spots due to the averaging of large OMI footprint. This effect is especially significant over Nanjing, as it is a local pollution hot spot surrounded by rather clean areas". If it is true, the NO2 measured by the MAX-DOAS is dominated by local emission. However the discussion on regional pollution transport in section 3.4, the author concludes that "the air quality of Nanjing is significantly influenced by the air pollution transportation, especially during

winter.". The two elaborations are contradictive. Therefore the authors need to carefully discuss the reason of the underestimations of the OMI NO2 data.

Response: The reviewer compares our estimation to previous study in Wuxi, China. We think that these studies cannot be compared directly for several reasons. There are major differences in satellite products used, measurement time and locations. In this study, we compare our MAX-DOAS measurements result to the NASA OMI NO2 standard product version 3 while the previous study in Wuxi used OMI NO2 product produced by KNMI. These products are processed with different algorithms, for example, there are significant differences in the spectral analysis, stratospheric and tropospheric NO2 separation methods, radiative transfer simulation and a priori profiles. Different versions of NASA OMI NO2 products even show a difference up to 40% (Krotkov et al., 2017), let alone the differences between two completely different algorithms. In addition, the differences in measurement time and location also make a big difference in the comparison. Measurements taken at the city center and several tens kilometer away in the suburban can already show a big difference.

To answer the reviewer question, whether the two OMI NO2 products are so different, we have also plotted the DOMINO version 2 data together with the NASA NO2 standard product in Figure 4. The result shows the NO2 VCD from the KNMI product is a factor of 2 higher than that of the NASA product. The result shows that the KNMI OMI product underestimated the NO2 VCDs by ~30% compared to the MAX-DOAS observations. This observation is consistence with the previous study. Further discussion is included in the manuscript (page 13, line 24-34).

We mentioned that regional transportation of pollutants has 'significant' impact on the local air quality which does not implies that regional transport is the 'major' source. Therefore, these sentences do not contradict with each other. Despite the strong local contribution, regional transportation of pollutants can also influence the local air quality. We have further clarified the confusion and rephrase the sentences in section 3.4 (page 18, line 20-21).

2) In section 3.4, the authors used the reconstructed maps to quantitatively validate the satellite maps. Therefore a speculated life time is used to scale MAX-DOAS VCD in the reconstruction of maps. However are the quantitative comparisons reasonable? Because the authors assume that all the pollutants measured by the MAX-DOAS instrument are from emissions in an area corresponding to the starting location of a trajectory. However emissions in different grids along the trajectory route should be mixed up and contribute to the pollutants measured by the MAX-DOAS in reality. The emissions from different distances should be scaled differently. But do we know the proportions of the different emissions? I think the reasonable comparisons of the re-constructed maps with the satellite maps are the relative distributions, but not the absolute values.

The reconstructed maps should depend on the selected backward time of trajectories. The author should show the maps with different trajectory backward time and compare them with the satellite maps in order to see which time is reasonable. And the suitable backward time depends on actual lifetime. Since the lifetime effect is already implied if different backward time is tested, the scaling with lifetime might be not needed and do not give any meaningful results. In addition, transports of pollutants can occur during night time and day time. Lifetime only matters for transports during day time. Nighttime transports can reach a far distance and contribute to concentrations of pollutants during day time. This is another reason why lifetime should not be applied.

The backward propagation method has been applied to long lifetime pollutants and also trace gases measured from MAX-DOAS in previous studies. Some references should be cited in the paper. Meanwhile the sentence "We developed a new technique to assemble the source contribution map using backward trajectory analysis" in the abstract might be inappropriate.

Response: We have to clarify that we did not perform any quantitative comparison between the MAX-DOAS and OMI datasets. We just wanted to remind the reader that there is a large difference in the MAX-DOAS and OMI VCDs. Therefore, the absolute value is expected to be different. Our discussion mainly focused on the spatial distribution of pollutant. We have rephrased the sentences to avoid any confusion (page 18, line 7-9).

I think there might be some misunderstandings with our approach. In our approach, NO2 and HCHO do not decay along the backward trajectory. The assumed lifetimes are only used to compute the weighting factors for the reconstruction of spatial distribution of NO2 and HCHO. As data are more reliable with shorter backward time, therefore, we give higher weight for data with shorter backward time. In order to avoid confusion, we have changed the term 'lifetime weight factor' to 'age weighting factor'. The age weighting approach is useful when multiple trajectories overlapping with each other within a single grid point. In addition, we did not mention that the pollutants measured by the MAX-DOAS are coming from primary emissions. They can also be secondary formed. We have only reconstructed the spatial distribution of pollutants, but not emission maps. In order to avoid the misunderstanding, we have further clarified this issue in the manuscript (page 16, line 6-8, page 17, line 1-2).

We understand that similar backward propagate methods have been used in some other study, we have implemented an age weighting scheme for the spatial distribution inversion, so that it fit better for the application on MAX-DOAS measurements. In order to avoid the confusion, we rephrased the sentences and added references to previous studies which use similar approach (page 15, line 16).

3) In section 3.5, the author compared the pollutants during the Youth Olympic Games with those before and after the event in order to characterize the effect of pollution control measures. Since pollution transports can impact Nanjing as the author demonstrates in section 3.4, the difference of transport conditions in the three periods should also be discussed. Meanwhile the author simply elaborates "As the meteorological conditions are very similar during the three periods". I think the author has to show wind fields, trajectories, precipitations, and temperatures in the three periods in order to convince the readers. Near-surface concentrations of the pollutants should be also derived from the MAX-DOAS profile inversion. Since near-surface concentrations should be mainly dominated by the local emission, but VCDs (AODs) contain contributions of pollutant transports. Therefore it is also meaningful to include the comparisons of the surface concentrations as VCDs shown in Fig.9.

Response: We have added the meteorological measurements such as temperature, wind speed and wind direction to support the discussion. The meteorological data are shown in Figure 10. A brief description of the meteorological data is added to section 2.3.

In addition, surface mixing ratios of NO2 and HCHO are now supplemented in Figure 9c. A more detailed discussion regarding the reduction of surface NO2 and HCHO concentration is included in section 3.5 (page 20, line 9, page 21, line 1-5).

Specific Comments:

1) P4 L3: A reference should be given for QDOAS. Please clarify which of the two wavelength ranges is used for NO2 and HCHO?

Response: We have supplemented the fitting range in the text (page 5, line 1-2) and cited reference for the use of QDOAS software (page 4, line 2).

2) P4 L4: Please clarify the reference spectrum is the zenith measurement in individual elevation scan or around noon time?

Response: We use the zenith spectrum taken in the same measurement cycle as reference in the analysis. This information is now supplied in the manuscript (page 5, line 2).

3) Table 1: Do you determine the DOAS fit settings based on sensitivity studies (which are not shown) or previous studies? If you determined them based on previous studies, some

references should be given. In addition, do you apply the wavelength dependent Ring suggested by Wagner et al., 2009? If not, please discuss why the additional Ring is not needed in your analysis. Wagner, T., Beirle, S., and Deutschmann, T.: Three-dimensional simulation of the Ring effect in observations of scattered sun light using Monte Carlo radiative transfer models, Atmos. Meas. Tech., 2, 113-124, 2009.

Response: The DOAS fit settings are taken from QA4ECV project and have been adopted for the CINDI-2 campaign. We have referred these DOAS fit settings to the previous study (page 5, line 7-10).

4) Section 2.1.2: examples of DOAS fits should be shown, especially for HCHO, in order to convince the quality of HCHO analysis.

Response: We have added an example of the DOAS fit as Figure 1. A brief description is also supplemented in the manuscript (page 5, line 10-12).

5) P4 L17-19: How do you filter the data under continuous clouds when the variability of O4 dSCDs are not large?

Response: Our cloud filtering approach is based on the analysis of the time series of O4 DSCD measured at each elevation. As O4 DSCDs are expected varying smoothly with time under clear sky condition, rapid change of O4 DSCDs are likely related to the present of cloud in the atmosphere. Therefore, we applied a high pass filter to the O4 DSCD time series to screen out cloud contaminated observations. The only limitation of this cloud screening algorithm is that the algorithm cannot distinguish continuous and homogeneous cloud condition. However, it is rare that the cloud does not change for a long time (within an hour) and the cloud layer is homogeneous for all viewing directions. We have also tried the color index method for cloud screening. However, the color index method tends to filter data will high aerosol load as the sky is whiter under high aerosol load condition. In addition, the aerosol load are usually high in Nanjing, the color index method identifies most of these high aerosol data as cloud contaminated. Therefore, we use the former high pass filter method for cloud screening in this study. We have supplemented the limitation of the cloud screening algorithm in section 2.1.1 (page 6, line 2-5).

6) P5 L15: Since O4 VCD can systematically vary during a year due to variations of temperature and pressure, as Wagner et al. (2018 AMT) demonstrated, the phenomenon can explain the scaling factor in many places. How do you consider the variation of temperatures in the retrievals of aerosols? If you don't consider it, a discussion on the uncertainties due to the effect has to be given.

Response: We use the U.S. standard mid-latitude atmosphere profiles for winter (January) and summer (July) and temporally interpolated to each month of the year for the radiative transfer simulation. This information is now supplemented in the manuscript (page 6, line 30-31)

7) P6 L11: How do you determine the single scattering albedo and asymmetry parameters, and also Ångström coefficient? The parameters can significantly change in the long-term measurements, uncertainty estimations of aerosol results due to the parameters should be given in the paper.

Response: These values are inherited from previous study. In order to investigate the uncertainty caused by the fixed set of aerosol optical properties, we performed sensitivity analysis using aerosol optical properties from the sun-photometer measurements in Nanjing and AERONET station ~150km southeast of the measurement site. The result shows that the uncertainty caused by Ångström coefficient, single scattering albedo and asymmetric parameter is ~2%, 1.5% and 4% respectively. This information is supplemented in the manuscript (page 7, line 27-30, page, line 29-31, page 11, line 1-5).

8) P6 L16-18: How do you determine the wavelengths of the AMF simulations of O4, NO2, and HCHO?

Response: We choose 360nm for the simulation of O4 DSCDs simply due the strong absorption at this wavelength. This wavelength is also commonly used in many studies for O4 simulations. As the NO2 DSCDs are also retrieved in the same fitting window, therefore, we adapted the same wavelength of 360nm for NO2 AMF simulation. For HCHO retrieval, our choice of AMF simulation wavelength of 340nm is close to the center wavelength of the DOAS fitting window of 342nm. This wavelength is also commonly used in HCHO retrieval, e.g., De Smedt et al., 2018.

9) P6 L20: How do you deal with the NO2 above 3km? The considerable amount of NO2 at high altitudes might also impact retrievals of NO2 below 3km.

Response: The MAX-DOAS measurements are not sensitive to higher altitudes. Therefore, we assume that the NO2 profile follows the US standard atmosphere. We have supplied this information in the manuscript (page 7, line 32).

10) Section 2.1.3: Figures of comparisons of measured dSCDs and modeled dSCDs for profile retrievals should be shown in the manuscript or supplement to show the convergence of the profile retrievals.

Response: We have added an example of aerosol, NO2 and HCHO profile retrieval in Figure 2.

11) Section 2.3: The overpass time of OMI should be given.

Response: We have now added the overpass time of OMI (page 9, line 22-23).

12) P8 L13-14: Can the constraint of a-priori profile contribute to the underestimations? In order to show this, comparisons of measured dSCDs and modeled dSCDs are needed.

Response: We have added an example of aerosol, NO2 and HCHO profile retrieval in Figure 2 which included measured and modeled DSCDs.

13) P8 L28: As I know, there are not domestic heating systems in Nanjing since it is in the south of Huai River.

Response: The reviewer is partly correct. There is no centralized heating system in Nanjing, but some of the new buildings are equipped with individual heating system with typically run on natural gas or electricity. Although the domestic heating emissions from southern part of China are smaller than that of the northern China, their contribution can still be significant. In order to avoid any confusion, we have rephrased the sentence in the manuscript (page 13, line 5-6).

14) P10, L1: The underestimation of OMI NO2 compared to MAX-DOAS is not consistent with Wang et al., 2017. The underestimation here is much stronger.

Response: See response to general comment 1.

15) P13, L6: Oxidation rate of VOCs to HCHO is also stronger in summer than in winter. The variations of oxidation rate can also contribute to seasonal pattern of HCHO. And secondary sources of HCHO are significant. The seasonal pattern of HCHO might be due to contributions of biogenic emissions of precursor VOCs. The sentence should be modified.

Response: We have revised the expression of the sentence and included the cause of higher oxidation rate of VOCs in summer (page 14, line 14-15)

16) P13, Figure 5: The color scale of subfigure (a) should be changed to allow seeing the gradient more clearly. As I elaborated in General comment (2), the relative distribution is much more important than the absolute values.

Response: We have adjusted the color scale of Figure 6 and 7.

17) P13, L16: Since you calculate the trajectories in each altitude grids of MAX-DOAS profiles, how do you combine the trajectories with the profiles? Do you assign partial columns in each vertical grid to different grid points in the map along trajectories at individual altitudes? The procedure need to be clarified.

Response: We have supplemented a more detailed description of the spatial reconstruction procedure (page 16, line 2-4).

18) P14, L5-6 how do you determine the lifetime and backward time? The question is corresponding to the general comment (2).

Response: See response to general comment 2.

19) P14, L12: As I demonstrate in comment (2), the quantitative comparisons with OMI data are not reasonable.

Response: See response to general comment 1.

20) P14, L19: Since HCHO is dominated by the secondary formations from VOCs, which have a long lifetime, therefore VOCs might be transported to a far distance and contribute to local HCHO concentrations. Therefore transport effects on HCHO might be even larger if the transports are from far distance. The backward time of trajectories of 6 hour might be not long enough in the reconstruction of HCHO maps. Following my general comment (2), I suggest you to generate the maps with different backward time of trajectories and compare the relative distributions with OMI maps.

Response: As discussed in response to general comment 2, we are not trying to reconstruct source map but the spatial distribution of HCHO. In addition, the lifetime is just used for the calculation of weighting factor. This approach is useful when multiple trajectories overlapping with each other within a single grid point. Of course we have looked into map with different backward time. As expected maps created with shorter backward time correlates better with OMI observations, but then the spatial coverage are very limited. In order to get a balance between having better spatial coverage and the reliability of the reconstructed pollution maps, these numbers are used in this study. This information is now added in the manuscript (page 17, line 7-8, page 18, line 1).

We thank reviewer #2 for the useful comments. These comments are helpful for improving our manuscript. We understand that the comments on the scientific content of the manuscript in general are positive, however, several clarifications are necessary. We have addressed the reviewer's comments on a point to point basis as below for consideration. All page and line numbers are refer to the marked-up version of the manuscript.

The manuscript entitled 'MAX-DOAS measurements of tropospheric NO2 and HCHO in Nanjing and the comparison to OMI observations' by Chan et al. presented a long term MAX-DOAS observations of atmospheric nitrogen dioxide (NO2) and formaldehyde (HCHO) in Nanjing. The MAX-DOAS measurements were validated by comparing to sun-photometer observations. The authors then used the MAX-DOAS data for the validation of the NASA's OMI NO2 and HCHO products. OMI observations in general show a good agreement with the ground based observations. A discussion of a priori profile on the satellite retrieval is also presented. The MAX-DOAS data is also used for the investigation of regional transportation of pollutants and for the assessment of air quality during the Youth Olympic Game in Nanjing. The study is in general well written and scientifically interesting for the community. Therefore, I recommend publishing the manuscript after addressed the following minor comments.

Minor comments:

1. Although the agreement between OMI and MAX-DOAS HCHO observations is already very good, it is still interesting to see the effect of MAX-DOAS profiles being used for OMI HCHO VCDs retrieval. I understand that there is a large fraction of HCHO above the MAX-DOAS retrieval height compared to NO2, using the MAX-DOAS profile would result in a larger OMI HCHO columns. This is also relevant for other MAX-DOAS satellite comparison studies.

Response: Following the reviewer's comment, we have added the OMI HCHO VCDs retrieved with MAX-DOAS measurements as a priori for comparison. The results are indicated in Figure 5. A more detailed discussion is added to the manuscript (page 14, line 19-26).

2. The authors mentioned on page 11 that it is difficult to quantify the effect of spatial inhomogeneity of NO2 on the satellite data comparison due to lack of high spatial resolution data. I am wonder if the MAX-DOAS is still measuring? If yes, then it would be useful to compare the latest measurement to TROPOMI observations. As TROPOMI provides much

higher spatial resolution data, these datasets are very useful for the quantification spatial gradient effect on satellite to ground based measurement comparison.

Response: Unfortunately, the MAX-DOAS measurements only cover a period from April 2013 to March 2017 while TROPOMI was launched in October 2017. The MAX-DOAS is under maintenance after March 2017 till now. Therefore, there is no overlap between the MAX-DOAS and TROPOMI data. We will try to the compare the MAX-DOAS data to TROPOMI observations when the MAX-DOAS is back online.

3. The reconstruction of spatial distribution NO2 and HCHO from MAX-DOAS measurements using trajectories simulations are particularly interesting. However, the description of the method is a bit too brief. The author should include a more detail description.

Response: We have supplemented a more detailed description of the spatial reconstruction procedure (page 16, line 2-8).

4. In addition, do the authors try other lifetime weight factors in this study? Are the weighting factors determined by fitting to satellite data or the authors just select a realistic one? This can be relevant for other similar studies.

Response: The assumed lifetime is only used for the calculation of the weighting factor and the weighting factor is only useful when multiple trajectories overlapping with each other within a single grid point. We have tried different lifetime and backward time to reconstruct the spatial distribution map of NO2 and HCHO. As expected maps created with shorter backward time correlates better with OMI observations, but then the spatial coverage are very limited. In order to get a balance between having better spatial coverage and the reliability of the reconstructed pollution maps, these number are used in this study. This information is now added in the manuscript (page 17, line 7-8, page 18, line 1).

5. Putting Figure 5 and Figure 7 a and b on the same page (or same figure) would be much easier for the readers to see the agreement between the reconstructed maps and satellite observations. Same comment applies to Figure 6 and Figure 7 c and d.

Response: We followed the reviewer's comment and combined Figure 5 and Figure 7 a and b as a single figure. Same procedure is also applied to Figure 6 and Figure 7 c and d.

6. Regarding to the assessments of air quality during Youth Olympic, it would be better to show some meteorological parameters during the 3 periods.

Response: We have added the meteorological measurements such as temperature, wind speed and wind direction to support the discussion. The meteorological data are shown in Figure 10. Description of the meteorological data can be found in section 2.3.

Technical comments:

1. Page 8, line 27: 'pNO2' should be 'NO2'

Response: We have corrected the typo.

2. Page14, line 12: 'This agree well with the fact' should be 'This agrees well with the fact'

Response: We have corrected the grammatical mistake.

3. There might still be other typos and errors in the manuscript. Please check the entire manuscript carefully.

Response: We have proofread the manuscript carefully to avoid any typo and error.

MAX-DOAS measurements of tropospheric NO$_2$ and HCHO in Nanjing and the comparison to OMI observations

Ka Lok Chan[1], Zhuoru Wang[1], Aijun Ding[2], Klaus-Peter Heue[1], Yicheng Shen[2], Jing Wang[3], Feng Zhang[4], Yining Shi[4], Nan Hao[5], and Mark Wenig[6]

[1]Remote Sensing Technology Institute (IMF), German Aerospace Center (DLR), Oberpfaffenhofen, Germany
[2]School of Atmospheric Sciences, Nanjing University, Nanjing, China
[3]Key Laboratory for Aerosol-Cloud-Precipitation of China Meteorological Administration, Nanjing University of Information Science and Technology, Nanjing, China
[4]Key Laboratory of Meteorological Disaster, Ministry of Education, Nanjing University of Information Science and Technology, Nanjing, China
[5]European Organisation for the Exploitation of Meteorological Satellites (EUMETSAT), Darmstadt, Germany
[6]Meteorological Institute, Ludwig-Maximilians-Universität München, München, Germany

Correspondence: Ka Lok Chan (ka.chan@dlr.de)

Abstract.

   In this paper, we present long term observations of atmospheric nitrogen dioxide (NO$_2$) and formaldehyde (HCHO) in Nanjing using a Multi-AXis Differential Optical Absorption Spectroscopy (MAX-DOAS) instrument. Ground based MAX-DOAS measurements were performed from April 2013 to February 2017. The MAX-DOAS measurements of NO$_2$ and HCHO vertical column densities (VCDs) are used to validate OMI satellite observations over Nanjing. The comparison shows that the OMI observations of NO$_2$ correlate well with the MAX-DOAS data with Pearson correlation coefficient (RR) of 0.91. However, OMI observations are on average a factor of 3 lower than the MAX-DOAS measurements. Replacing the a priori NO$_2$ profiles by the MAX-DOAS profiles in the OMI NO$_2$ VCD retrieval would increase the OMI NO$_2$ VCDs by ∼30 % with correlation nearly unchanged. The comparison result of MAX-DOAS and OMI observations of HCHO VCD shows a good agreement with R R of 0.75 and the slope of the regression line is 0.99. ~~We developed a new technique to assemble the source contribution map using backward trajectory analysis. The~~ An age weighted backward propagation approach is applied to the MAX-DOAS measurements of NO$_2$ and HCHO to reconstruct the spatial distribution of NO$_2$ and HCHO over ~~the~~ Yangtze River Delta during summer and winter time. The reconstructed NO$_2$ fields show a distinct agreement with OMI satellite observations. However, due to the short atmospheric lifetime of HCHO, the backward propagated HCHO data does not show a strong spatial correlation with the OMI HCHO observations. The result shows the MAX-DOAS measurements are sensitive to the air pollution transportation in the Yangtze River Delta, indicating the air quality in Nanjing is significantly influenced by regional transportation of air pollutants. The MAX-DOAS data are also used to evaluate the effectiveness of air pollution control measures implemented during the Youth Olympic Games 2014. The MAX-DOAS data show a significant reduction of ambient aerosol, NO$_2$ and HCHO (30 % - 50 %) during the Youth Olympic Games. Our results provide a better understanding of the transportation and sources of pollutants in over the Yangtze River Delta as well as the effect of emission control measures during large international event, which are important for the future design of air pollution control policies.

1 Introduction

Nitrogen dioxide (NO_2) and formaldehyde (HCHO) are major atmospheric pollutants playing crucial roles in atmospheric chemistry. NO_2 is a catalyst for ozone (O_3) formation in the troposphere, while also participating in the catalytic destruction of stratospheric O_3 (Crutzen, 1970). Major NO_2 sources include fossil fuel combustion, biomass burning, lightning and oxidation of ammonia (Bond et al., 2001; Zhang et al., 2003). The emissions of NO_2 show a significant increasing trend in China due to the rapid industrialization and economy development in the last two decades (Zhang et al., 2007; van der A et al., 2008; Zhao et al., 2013), making it one of the most severe air pollution problems. HCHO is an intermediate product of the oxidation of almost all volatile organic compounds (VOCs). Therefore, it is widely used as an indicator of non methane volatile organic compounds (NMVOCs) (Fried et al., 2011). VOCs also have significant impacts on the abundance of hydroxyl (OH) radicals in the atmosphere, which is the major oxidant in the tropospheric. Major HCHO sources over the continents include the oxidation of VOCs emitted from plants, biomass burning, traffic and industrial emissions. Oxidation of methane (CH_4) emitted from the ocean is the main source of HCHO over water. Both NO_2 and HCHO contribute to the formation of secondary aerosols (Jang and Kamens, 2001) and they are toxic to human in high concentration. The spatial distribution of NO_2 and HCHO is strongly related to their emissions due to their short atmospheric lifetime. Consequently, it is important to understand the spatial and temporal variations of atmospheric NO_2 and HCHO for better air pollution management and control.

Multi-AXis Differential Optical Absorption Spectroscopy (MAX-DOAS) is a powerful remote sensing measurement technique which provides valuable vertical distribution information of atmospheric aerosols and trace gases (Platt and Stutz, 2008). Information of tropospheric aerosols and traces gases are obtained from the molecular absorption in the ultraviolet and visible spectral bands by applying the differential optical absorption spectroscopy (DOAS) technique to the observations of scattered sun light spectrum in several different viewing directions. As the experimental setup of MAX-DOAS is rather simple and inexpensive, it has been widely used for the observation of atmospheric aerosols and trace gases in the past decade (Hönninger and Platt, 2002; Hönninger et al., 2004; Wittrock et al., 2004; Frieß et al., 2006; Irie et al., 2008; Li et al., 2010; Clémer et al., 2010; Halla et al., 2011; Li et al., 2013; Ma et al., 2013; Chan et al., 2015; Jin et al., 2016; Wang et al., 2016; Chan et al., 2018). MAX-DOAS measurements are highly sensitive to aerosols and trace gases in the lower troposphere and provide valuable information of the vertical distribution of aerosol extinction and trace gases. The information of the aerosol and trace gas vertical profiles are particularly important for the study of the physical and chemical processes in the atmosphere.

Satellite based remote sensing measurements provide indispensable spatial information of air pollutants (Burrows et al., 1999; Bovensmann et al., 1999; Callies et al., 2000; Levelt et al., 2006). Trace gas columns are derived from the satellite observations of Earth's reflected solar spectrum for the investigation of atmospheric dynamics and emissions from both anthropogenic and natural sources (Beirle et al., 2003; Wenig et al., 2003; Beirle et al., 2004; Richter et al., 2005; Zhang et al., 2007; van der A et al., 2008). Satellite measurements can also be used to determine the effectiveness of emission control measures (Mijling et al., 2009; Witte et al., 2009; Wu et al., 2013; Chan et al., 2015). However, the uncertainties of satellite trace gas column retrieval are strongly dependent on the accuracy of the assumptions of trace gas vertical distributions. In addition, the temporal resolution of satellite measurements is often limited to single observation per day. Therefore, it is useful to compare

and integrate ground based and satellite observations for the interpretation of the spatial and temporal variation of NO_2 and HCHO.

Nanjing is the second largest city in the Yangtze River Delta and Eastern China. It is also the provincial capital of Jiangsu province. The population of Nanjing is about 8 million. Yangtze River is running through the city of Nanjing making it the largest inland port in China. Industrial, water and road transportation are the major anthropogenic sources of air pollutions in Nanjing. Due to its rapid development as well as its surrounding cities in the Yangtze River Delta, Nanjing is facing a series of air pollution problems in recent years. In addition, Nanjing has also hosted several important international events including the summer Youth Olympic Games in 2014. Therefore, it is important to have a better understanding of the air pollution sources in order to support the design of air quality related environmental policies in the future.

In this paper, we present long term MAX-DOAS observations of NO_2 and HCHO in Nanjing. Ground based MAX-DOAS measurements were performed from April 2013 to February 2017. Details of the MAX-DOAS experimental setup, the spectral analysis as well as the retrieval of the aerosol extinction, NO_2 and HCHO profiles are presented in section 2. Section 3.1 shows the validation of MAX-DOAS aerosol observations by comparing the reported aerosol optical depths (AODs) to sun photometer measurements. The comparison of NO_2 and HCHO VCDs measured by the MAX-DOAS and OMI satellite is presented in Section 3.2. An analysis of regional transport of pollutants over Yangtze River Delta is shown in section 3.4. In section 3.5, we presented an evaluation of the pollution reduction observed during the Youth Olympic Games in 2014.

2 Methodology

2.1 MAX-DOAS measurements

2.1.1 Experimental setup

A MAX-DOAS instrument was set up at a meteorological station of Nanjing University (32.12°N, 118.95°E) which is located on a small hill in the University campus at about 45 m above sea level. The meteorological station is located about 17 km northeast of the Nanjing city center and about 5 km south of the Yangtze River. The MAX-DOAS instrument for scattered sun-light measurements consists of a scanning telescope, a stepping motor controlling the viewing zenith angle of the telescope and a spectrometer. Scattered sun-light collected by the telescope is redirected by a quartz fiber to the spectrometer for spectral analysis. The field of view of the telescope is about 0.6°. An Ocean Optic USB2000 spectrometer equipped with a Sony ILX511 charge-coupled device (CCD) detector is used to cover the wavelength range from 288 nn to 434 nm. The full width half maximum (FWHM) spectral resolution of the spectrometer is 0.6 nm (at 360 nm).

A complete measurement cycle consists of scattered sun-light observations at elevation angle (α) of 1°, 2°, 3°, 6°, 10°, 18°, 30° and the zenith (90°). The viewing azimuth angle is adjusted to 320° (northwest). The exposure time and the number of scan of each measurement is adjusted automatically depending on the received intensity of the scattered sun-light spectrum in order to achieve a similar intensity level for all the measurements. A full measurement sequence takes about 5 - 10 minutes.

2.1.2 Spectral retrieval
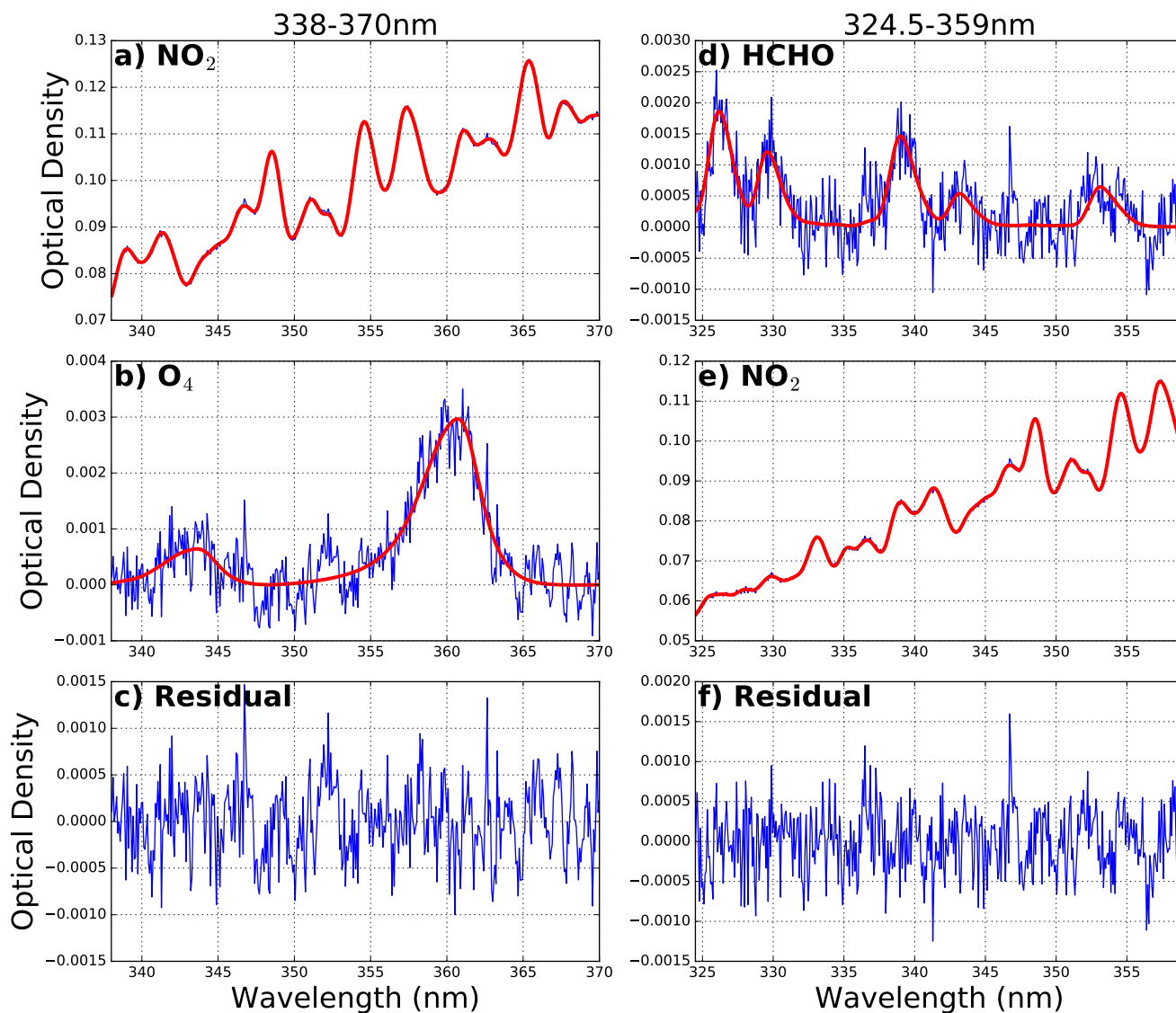
Figure 1. An example of the DOAS retrieval of NO_2 and HCHO DSCDs from a a MAX-DOAS spectrum taken on 12th May 2013 at 08:48 (local time) with viewing elevation angle of $1°$. The left panels show the DOAS fit in the wavelength range of 338 - 370 nm, while the right panels show DOAS fit in the wavelength range of 324.5 - 359 nm.

All the measurement spectra were first corrected for offset and dark current and then analyzed using the spectral analyzing software QDOAS (version 3.2 (http://uv-vis.aeronomie.be/software/QDOAS/). The MAX-DOAS spectral fit was performed at

2 different wavelength ranges ~~for the retrieval of~~ of 338 - 370 nm for NO_2 ~~and HCHO~~retrieval and 324.5 - 359 nm for HCHO retrieval. In this study, the zenith spectrum ($\alpha = 90°$) taken in the same measurement cycle is used as reference spectrum in the spectral analysis to retrieve the differential slant column densities (DSCDs). The differential slant column density (DSCD) is defined as the difference between the slant column density (SCD) of the measured spectrum and the corresponding zenith reference spectrum. The broad band spectral structures caused by Rayleigh and Mie scattering are removed by including a low order polynomial in the DOAS fit. Absorption cross section of several trace gases were included in the DOAS fit at different fitting ranges, details of the DOAS retrieval settings for each wavelength range are listed in Table 1. The DOAS fit settings follow the one used in the Quality Assurance for Essential Climate Variables (QA4ECV) project (http://www.qa4ecv.eu/). These settings have also been adopted for the Second Cabauw Intercomparison campaign for Nitrogen Dioxide measuring Instruments (CINDI-2) campaign (http://www.tropomi.eu/data-products/cindi-2). Small shift and squeeze of the wavelengths are allowed in the wavelength mapping process in order to compensate small uncertainties caused by the instability of the spectrograph. Figure 1 shows an example of the spectral fit retrieval of NO_2 and HCHO DSCDs from a MAX-DOAS spectrum taken on 12th May 2013 at 08:48 (local time) with viewing elevation angle of $1°$.

Table 1. The DOAS retrieval settings for different wavelength bands.

Species	Temperature	Wavelength Range		Reference
		324.5 - 359 nm	338 - 370 nm	
BrO	223 K	✓	✓	Fleischmann et al. (2003)
HCHO	298 K	✓	✓	Meller and Moortgat (2000)
NO_2 [a]	298 K	✓	✓	Vandaele et al. (1998)
NO_2 [a]	220 K		✓	Vandaele et al. (1998)
O_3 [b]	223 K	✓	✓	Serdyuchenko et al. (2014)
O_3 [b]	243 K	✓	✓	Serdyuchenko et al. (2014)
O_4	293 K	✓	✓	Thalman and Volkamer (2013)
Ring		✓	✓	
Polynomial		5th order	5th order	

[a] I_0 correction is applied with SCD of 10^{17} molec/cm^2 (Aliwell et al., 2002).

[b] I_0 correction is applied with SCD of 10^{20} molec/cm^2 (Aliwell et al., 2002).

As clouds are not included in the radiative transfer calculation of the aerosol and trace gas profile retrieval, the retrieval result can be significantly influenced by the present of cloud in the atmosphere. Therefore, the retrieved DSCDs were first filtered by removing cloudy scenes before proceeding to the aerosol and trace gas profile retrieval. The vertical profile of the oxygen collision complex O_4 only varies in a small range with atmospheric pressure and temperature, the retrieved O_4 DSCDs and (relative) intensities are assumed to vary smoothly with time with the solar and viewing geometry. Rapid change of O_4 DSCDs and intensities indicates a sudden change in the radiative transport condition which is likely due to the present of clouds. Therefore, we applied a locally weighted regression smoothing filter (LOWESS) (Cleveland, 1981) with a regression window

of 3 hours to the O_4 DSCDs and intensities time series at each elevation angle to filter data influenced by inhomogeneous and/or rapid changes of radiation transport conditions. Data with fast varying O_4 DSCDs and intensities were filter out. Only data with slow varying O_4 DSCDs and intensities were used in the aerosol and trace gas retrieval. The limitation of this cloud screening algorithm is that the algorithm is not able to distinguish continuous and homogeneous cloud condition. However,

5 it is rare that the cloud does not change for a long time (within an hour) and the cloud layer is homogeneous for all viewing directions.

2.1.3 Aerosol and trace gas profile retrieval

Previous studies show that there is a systematic discrepancy between observation and model simulation of O_4 DSCDs (Wagner et al., 2009; Clémer et al., 2010; Wagner et al., 2011; Chan et al., 2015; Wang et al., 2016; Chan et al., 2018; Zhang et al., 2018).

10 A scaling correction factor has to be applied to the measured O_4 DSCDs in order to bring measurement and model results into agreement. However, the physical meaning of this observation is still not well understood (Ortega et al., 2016; Wagner et al., 2018)(Ortega e Theoretically, the optical path should be the longest under aerosol free condition for off zenith measurement. Thus, the MAX-DOAS measurement of O_4 DSCDs should be smaller than the one simulated with pure Rayleigh atmosphere. In this study, we compared the forward simulation of O_4 DSCDs under aerosol free condition to the O_4 DSCDs retrieved from the MAX-DOAS

15 observations to examine the necessity of O_4 correction. Our result shows that the measured O_4 DSCDs occasionally exceeded the forward simulation results which implies that correction of O_4 DSCDs is necessary. The ratio between simulated and measured O_4 DSCD varies from 0.75 to 1.0 for cases where the measured O_4 DSCDs exceeded the forward simulation results. Our finding agrees with previous reported scaling correction factors of O_4 DSCDs which is ranging from 0.7 up to 1.0. In order to avoid over-correction due to the outliers, we take the 10th 10th percentile instead of the minimum value of the simulated and

20 measured O_4 DSCD ratio as the correction factor which is ~ 0.8. All MAX-DOAS observations of O_4 DSCD are corrected by multiplying the correction factor of 0.8. From hereafter, all O_4 DSCDs are referring to the corrected O_4 DSCDs.

The conversion of the MAX-DOAS observations to aerosol extinction and trace gas profile requires inversion of the underlying radiative transfer equations. These equations cannot be linearized, therefore, it is suggested to fit the measurement quantities to the forward calculation of radiation transfer (Wagner et al., 2004; Hönninger et al., 2004; Sinreich et al., 2005;

25 Frieß et al., 2006; Hartl and Wenig, 2013; Chan et al., 2018). As the vertical distribution profile of O_4 is very stable and it has several absorption bands in the ultraviolet and visible spectral range, it is commonly used as fitting quantity for the aerosols retrieval.

In this study, aerosol vertical profiles are retrieved at the 360 nm O_4 absorption band using the Munich Multiple wavelength MAX-DOAS retrieval algorithm (M^3) (Chan et al., 2018). The algorithm is developed based on the optimal estimation

30 method (Rodgers, 2000) and utilizes the Library for Radiative Transfer (LibRadTran) model (Emde et al., 2016) as the forward model. In this study, the U.S. standard mid-latitude atmosphere profiles for winter (January) and summer (July) are temporally interpolated to each month of the year for the radiative transfer simulations. A brief description of the aerosol and trace gases vertical profile retrieval algorithm and the parameterization used in this study are presented in the following. A more detailed description of the 3M retrieval algorithm can be found in Chan et al. (2018).

In this study, all valid MAX-DOAS observations within a single measurement cycle are grouped together for the aerosol vertical profile retrieval. Assuming the set of measurement can be reproduced by the forward model and the forward model results are dependent on the aerosol extinction profile, we can then retrieve the aerosol extinction profile by fitting the forward model results to the MAX-DOAS O_4 observations using the iterative Newton-Gauss method. As the information contained in the MAX-DOAS observations are most likely not enough to retrieve an unique aerosol extinction profile, we have to supply the necessary information to the aerosol inversion in a form of a priori aerosol profile. As the aerosol load in Nanjing varies in a wide range, using a fix a priori could result in over regularizing the retrieval under higher aerosol load conditions. Therefore, we have implemented an iterative approach to avoid over regularizing the retrieval. We first use a fixed initial a priori to retrieve the aerosol extinction profile. The fixed a priori profile is then scaled to have the same aerosol optical depth retrieved from the previous run. Then the new a priori is used in the next run to retrieve the aerosol extinction profile. This procedure is repeated until the difference between the retrieved and a priori aerosol optical depth is less than 10 % or the number of iteration reaches the limit.

As aerosols are typically emitted and formed close to the surface in urban areas, we assume the a priori aerosol extinction profile follows an exponentially decreasing function with a scale height of 1.0 km. The aerosol optical depth (AOD) of the a priori aerosol profile is set to 0.5 for the retrieval at 360 nm. The uncertainties of the a priori aerosol profile are set to 100 % and the correlation length of the aerosol inversion is assumed to be 0.5 km. As MAX-DOAS measurements are more sensitive to the aerosol and trace gases close to the instrument, therefore, we divided the lowest 3.0 km of the troposphere into 15 layers with thickness of each layer of 200 m. A fix set of single scattering albedo of 0.92, asymmetry parameter of 0.68 and ground albedo of 0.04 is assumed in the radiative transfer calculations. An example of aerosol extinction profile retrieval is indicated in Figure 2a-c.

The aerosol information obtained from the procedure described above were used for the differential box air mass factor (ΔDAMF) calculation for the trace gas profile inversion. The ΔDAMFs were calculated at a single wavelength for the retrieval of trace gas profile using the radiative transfer model LibRadTran with the Monte Carlo simulation module MYSTIC (Emde et al., 2016). The ΔDAMF was assumed to be constant within the DOAS spectral fitting windows. In this study, vertical distribution profiles of NO_2 are retrieved at 360 nm. An example of NO_2 profile retrieval is indicated in Figure 2d-f. For HCHO vertical distribution profile retrieval, aerosol extinction profiles obtained at the 360 nm O_4 band are converted to 340 nm assuming a fixed Ångström coefficient (Ångström, 1929) of 1. The Ångström coefficient can varies significantly with time. Sun photometer measurements in Nanjing (see Section 2.2) show that the Ångström coefficient mostly varies between 0.7 (10th percentile) and 1.4 (90th percentile). Based on the sun photometer observations, we estimated the error caused by fixed Ångström coefficient on aerosol extinction is less than 2 %. The ΔDAMFs are subsequently calculated at 340 nm for the HCHO profile retrieval. An example of HCHO profile retrieval is indicated in Figure 2g-i.

The atmosphere layer settings of the trace gas profile retrieval are the same as the one used in the aerosol profile retrieval. NO_2 and HCHO concentrations above the retrieval height (3 km) are assumed to follow the U.S. standard atmosphere. As the trace gas profile cannot be fully reconstructed by the small number of measurements, therefore, we use the optimal estimation method (Rodgers, 2000) with iterative approach to regularize the inversion (Chan et al., 2015, 2018). The first step uses a
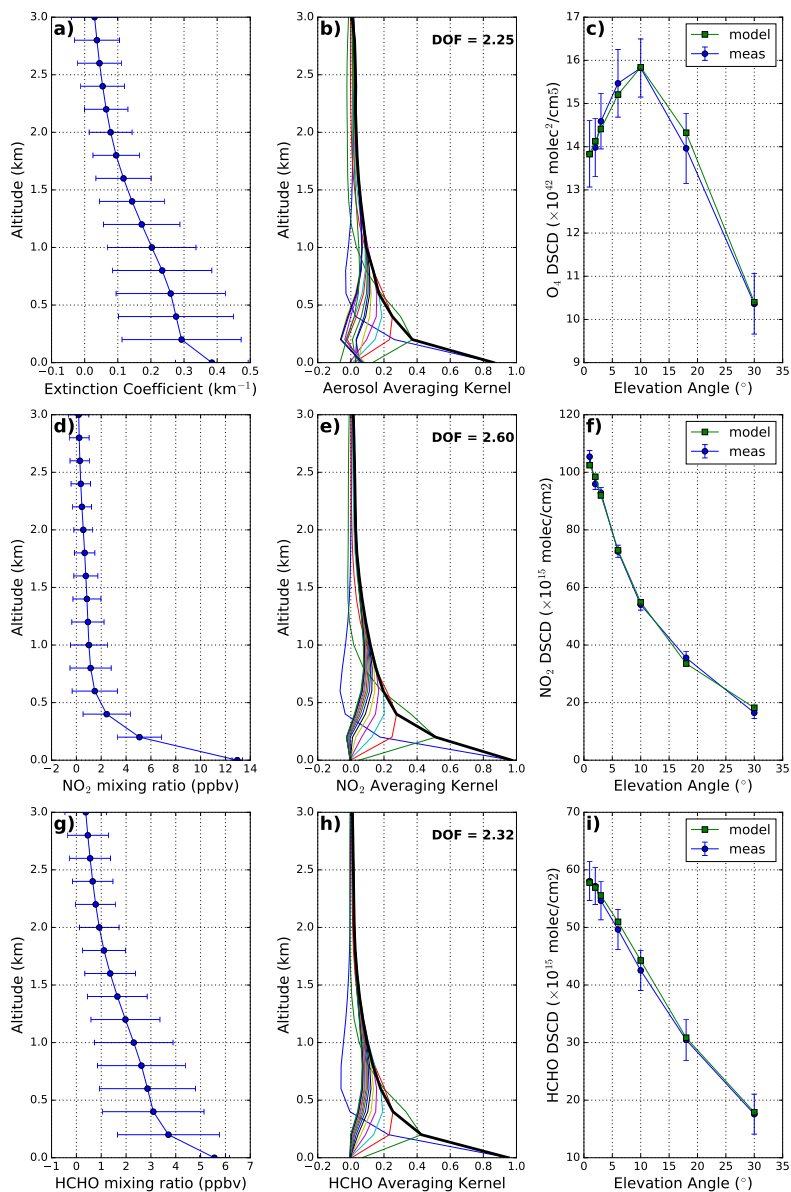
Figure 2. An example of vertical profile retrieval of aerosol extinction, NO_2 and HCHO from MAX-DOAS measurements taken on 4th July 2013 at around 8:47 (local time). The left panels show the (a) aerosol extinction, (d) NO_2 and (g) HCHO profiles. Panels in the middle column indicate the average kernel of (b) aerosol extinction, (e) NO_2 and (h) HCHO profile retrieval. The measured (blue curves) and modeled (green curves) DSCDs of (c) O_4, (f) NO_2 and (i) HCHO are shown in the right column.

fixed initial a priori to retrieve the trace gas distribution. The fixed a priori profile is then scaled to have the vertical column retrieved from the first run. The scaled a priori is used in the next run to retrieve the trace gas profile. The process repeats until

the difference between the retrieved and a priori trace gas vertical column is less than 10 % or the number of iteration reaches the limit. In this study, the a priori is assumed to follow an exponential decrease function with a scale height of 1.0 km. The uncertainty of the a priori profile is set to 100 % of the a priori and correlation length is set to 0.5 km in the trace gas profile inversion. The NO_2 vertical column density (VCD) of the a priori is set to 2×10^{16} molec/cm^2 while the a priori HCHO VCD is set to 1×10^{16} molec/cm^2.

2.2 Sun photometer measurements

A sun photometer was installed on the roof of a building of Nanjing University of Information Science and Technology (32.20°N, 118.70°E), which is located at the north bank of the Yangtze River. The sun photometer site is ∼25 km northwest of the MAX-DOAS measurement site. The two instruments are separated by the Yangtze River. An industrial park is about 3 km east of the sun photometer site. Heavy industry factories, i.e., steel and cement plants are located in the industrial park. In this study, AODs measured by the sun photometer were used for the inter-comparison study to validate the MAX-DOAS aerosol retrieval. Cloud screened data were used. The data consist of AOD measurements at 7 different wavelength channels from 340 nm to 1020 nm. AOD measurements at 340 nm and 380 nm are interpolated to 360 nm for comparison.

2.3 ~~OMI Satellite observations~~Meteorological data

Meteorological parameters such as temperature, wind speed and wind direction are taken from a weather station in Nanjing which is located about 20 km south of the MAX-DOAS measurement site. The weather station is operated by the National Meteorological Center of China Meteorological Administration. These data are available on the webpage of China Meteorological Administration (https://data.cma.cn/site/index.html). The meteorological data are mainly used for the analysis of meteorological effects on air quality in Nanjing during the Youth Olympic Games in 2014.

2.4 OMI satellite observations

The Ozone Monitoring Instrument (OMI) is a passive nadir-viewing satellite borne imaging spectrometer (Levelt et al., 2006) on board the Earth Observing System's (EOS) Aura satellite. The EOS Aura satellite orbit at an altitude of ∼710 km with a local equator overpass time of 13:45 LT (local time). The instrument consists of two charge-coupled devices (CCDs) covering a wavelength range from 264 nm to 504 nm. A scan provides measurements at 60 positions across the orbital track covering a swath of approximately 2600 km. The spatial resolution of OMI varies from ∼320 km^2 (at nadir) to ∼6400 km^2 (at both edges of the swath). The instrument scans along 14.5 sun-synchronous polar orbits per day providing daily global coverage.

The NASA's OMI NO_2 and HCHO standard product version 3 (Krotkov et al., 2017; González Abad et al., 2015) are used in this study. In the NO_2 product, the slant column densities (SCDs) of NO_2 are derived from Earth's reflected spectra in the visible range (402 - 465 nm) using an iterative sequential algorithm (Marchenko et al., 2015). Previous studies show the updated SCDs are on average 10 - 40 % lower compared to the previous version of retrieval (Marchenko et al., 2015). The OMI NO_2 SCDs are converted to VCDs by using the concept of air mass factor (AMF) (Solomon et al., 1987). The AMFs are calculated

using NO$_2$ profile simulated by the Global Modeling Initiative (GMI) chemistry transport model. The horizontal resolution of GMI is 1° (latitude) × 1.25° (longitude) (Rotman et al., 2001). Separation of stratospheric and tropospheric columns is achieved by the local analysis of the stratospheric field over unpolluted areas (Bucsela et al., 2013).

The OMI HCHO retrieval algorithm uses the direct fit of radiances in the spectral range from 328.5 nm to 356.5 nm for the SCD retrieval. In the current version of HCHO product, OMI radiance measurement over the remote Pacific is used as reference in the fitting process. This approach is reported to reduce the interferences from unresolved spectral structures in the retrieval of weak absorbers like HCHO (De Smedt et al., 2018). The retrieved SCDs are then converted to VCDs using the AMF approach. The AMFs are calculated based on climatological HCHO profiles.

2.5 Back trajectory modeling

The National Oceanic and Atmospheric Administration Air Resources Laboratory (NOAA ARL) developed HYbrid Single Particle Lagrangian Integrated Trajectory (HYSPLIT) model (Stein et al., 2015) (http://www.arl.noaa.gov/HYSPLIT.php) was used to investigate the transportation pollutants over Yangtze River Delta. Meteorological data from the Global Data Assimilation System (GDAS) with a spatial resolution of 0.5° × 0.5° and 24 vertical levels was used in the model for trajectory simulations. Backward trajectories are computed for air masses arriving at the mid point of each MAX-DOAS retrieval layer.

3 Results and discussions

3.1 Compariosn of MAX-DOAS and sun photometer AODs

Aerosol optical depths (AODs) retrieved from the MAX-DOAS observations are compared to the sun photometer measurements. As the sampling resolution of the MAX-DOAS and the sun photometer are different, individual measurements are averaged to hourly, daily and monthly values for comparison. Figure 3 shows the scatter plot of AOD measured by the sun photometer and MAX-DOAS. Both datasets are cloud filtered. AODs measured by both MAX-DOAS and sun photometer are in general in good agreement. The Pearson correlation coefficient (RR) of daily averaged data is 0.73. The slope of the total least squares regression between the two datasets is 0.56 with an offset of 0.13. The discrepancies between the two datasets can be explain by the difference of measurement technique and measurement location. The sun photometer derives AOD from direct sun measurements, while the MAX-DOAS retrieves AOD using the O$_4$ absorption information from scattered sun light. The sun photometer is sensitive to the entire column while the MAX-DOAS is mostly sensitive to aerosol at the lowest few kilometers of the troposphere. Therefore, the MAX-DOAS is likely to underestimate the AOD when there is an elevated aerosol layer in the upper troposphere. This explanation matches with the observations that the MAX-DOAS agrees better with the sun photometer under low aerosol conditions (AOD < 1) and underestimate the AOD during high AOD conditions. Another source of error is the assumption of aerosol optical properties in the MAX-DOAS retrieval. In order to quantify the error caused by the fixed asymmetry parameter and single scatter albedo used in the aerosol retrieval, we have performed a sensitivity analysis by retrieving the aerosol profile with different asymmetry parameter and single scattering albedo. As the

10
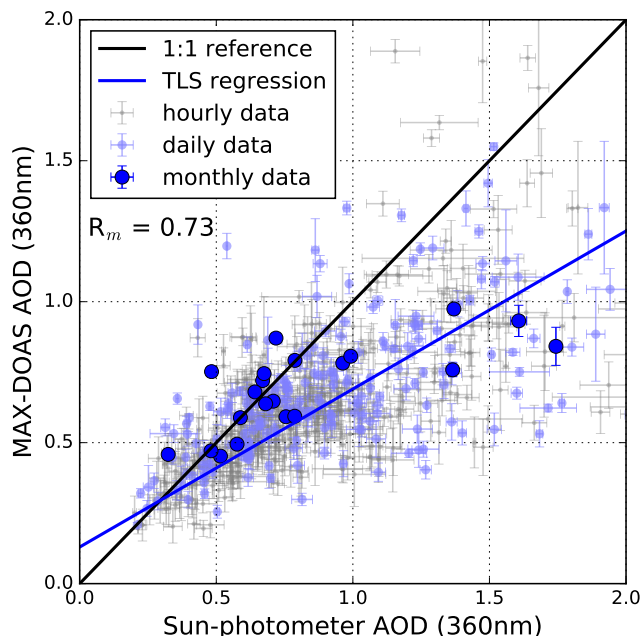
Figure 3. Comparison of AOD measured by the MAX-DOAS and sunphotometer. The total least squares regression line is calculated based on the daily data.

sun photometer in Nanjing does not provide full inversion of aerosol optical properties, aerosol optical properties are taken from the Taihu AERONET station which is about 150 km southeast of Nanjing. The 10th and 90th percentile of asymmetry parameter and single scatter albedo are used for the sensitivity study. The result shows that the error caused by the fixed asymmetry parameter on AOD retrieval can be up to 4 %, which the single scattering albedo shows a smaller impact of up to 1.5 %. In addition, the MAX-DOAS and sun photometer are separated by a distance of ~25 km and the sun photometer site is very close to an industrial park, where the heavy polluted industries are located, i.e., steel and cement plants. Therefore, the sun photometer measurements are expect to be higher than the MAX-DOAS observations. Accounting for these effects, the MAX-DOAS and sun photometer observation agrees well with each other and the MAX-DOAS derived aerosol profiles are reliable for the retrieval of NO_2 and HCHO profiles.

3.2 Comparison of MAX-DOAS and OMI observations

Vertical column densities of NO_2 and HCHO retrieved from the ground based MAX-DOAS measurements are compared to OMI satellite observations. MAX-DOAS data are temporally averaged around the OMI overpass time from 12:00 to 14:00 (local time), while OMI VCDs are spatially averaged for pixels within 20 km of the MAX-DOAS measurement site. Time series of MAX-DOAS and OMI observations of NO_2 and HCHO VCDs are shown in Figure 4 and Figure 5, respectively. Both

11
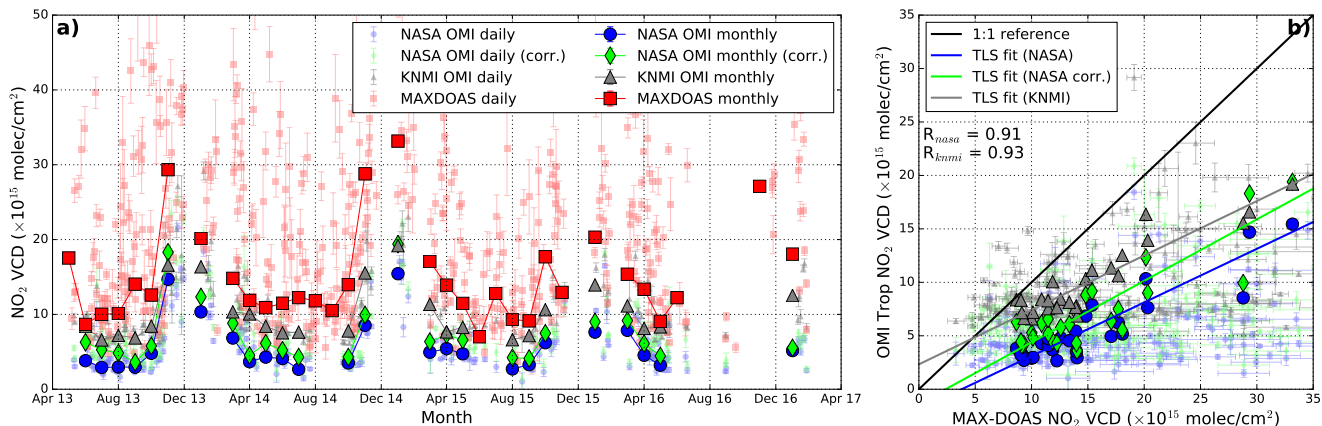
Figure 4. (a) Time series of the MAX-DOAS (red markers) and NASA's OMI (blue markers) tropospheric NO$_2$ VCDs over Nanjing from 2013 to 2017. MAX-DOAS data are temporally averaged around the OMI overpass time. OMI measurements are spatially averaged for pixels within 20 km of the MAX-DOAS measurement site. OMI NO$_2$ VCDs retrieved using MAX-DOAS profile as a priori information are indicated as green markers. Tropospheric NO$_2$ VCDs taken from KNMI product are also shown as gray marker for reference. (b) Comparison of tropospheric NO$_2$ VCDs between the MAX-DOAS and OMI satellite observations. The total least squares regression line is calculated based on the monthly average data.
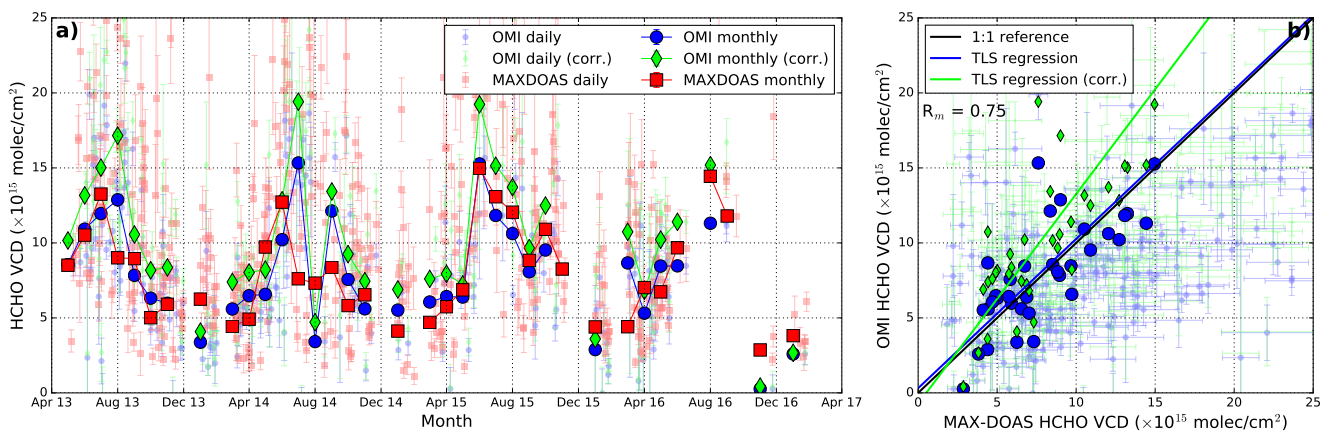
Figure 5. (a) Time series of the MAX-DOAS (red markers) and OMI (blue markers) HCHO VCDs over Nanjing from 2013 to 2017. MAX-DOAS data are temporally averaged around the OMI overpass time. OMI measurements are spatially averaged for pixels within 20 km of the MAX-DOAS measurement site. OMI NO$_2$ VCDs retrieved using MAX-DOAS profile as a priori information are indicated as green markers. (b) Comparison of HCHO VCDs between the MAX-DOAS and OMI satellite observations. The total least squares regression line is calculated based on the monthly average data.

12

OMI NO_2 and HCHO datasets are filtered for cloud radiance fraction smaller than 0.4. Daily and monthly averaged data are shown. Missing data for some months are due to cloud filtering or instrumental issues of the MAX-DOAS.

~~pNO~~NO_2 VCDs measured by the MAX-DOAS and the OMI satellite shows a similar seasonal pattern with higher NO_2 columns during winter and lower NO_2 values over summer. Higher NO_2 levels are due ~~to higher domestic heating emissions~~
5 ~~and~~ longer atmospheric lifetime of NO_2 during winter ~~. The~~ and higher emissions in winter, e.g., higher power consumption and emissions from individual domestic heating. MAX-DOAS and OMI observations show good temporal consistency with each other with Pearson correlation coefficient (~~R~~R) of 0.91. Despite the strong correlation between the two datasets, the OMI observations is systematically underestimating the NO_2 columns. The slope and offset of the total least squares regression between the two datasets is 0.50 and -1.89×10^{15} molec/cm^2, respectively. Averaged OMI NO_2 column over Nanjing is
10 5.67×10^{15} molec/cm^2 which is about ~~a factor 3~~ 60 % lower than the MAX-DOAS averaged VCD of 14.96×10^{15} molec/cm^2 (see Figure 4). The underestimation of NO_2 VCDs from OMI measurements agree with previous studies in the Yangtze Delta ~~(Chan et al., 2015; Wang et al., 2017)~~(Chan et al., 2015). The discrepancies ~~are mainly~~ can be related to the differences in spatial coverage between the ground based and satellite observations and the uncertainties related to the NO_2 vertical distribution profile shape used in the air mass factor calculation. We quantified the influence of NO_2 vertical distribution profile on the
15 air mass factor calculation by recomputed the OMI tropospheric NO_2 air mass factor using the MAX-DOAS NO_2 profile as a priori information. OMI NO_2 VCDs retrieved with MAX-DOAS NO_2 profiles are also indicated in Figure 4. Using the MAX-DOAS profile as a priori information in the OMI NO_2 VCDs retrieval on average increased the OMI NO_2 VCDs by $\sim$30 % with correlation nearly unchanged. The averaged OMI NO_2 column over Nanjing increased to 7.29×10^{15} molec/cm^2. In addition, the slope of the regression line increases from 0.50 to 0.57 while the offset reduces from -1.89 to -1.35×10^{15} molec/cm^2.
20 The result indicates that a better estimation of NO_2 vertical distribution in the satellite VCD retrieval reduces the discrepancies. Our findings agree with previous studies that using better estimated NO_2 vertical profile in the satellite air mass factor calculation enhanced the OMI NO_2 columns and reduced discrepancies between OMI and ground based observations (Chan et al., 2012; Lin et al., 2014; Chan et al., 2015; Wang et al., 2017). However, the improved OMI NO_2 VCDs are still about ~~a factor of 2~~ 50 % lower than the MAX-DOAS observations indicating that there are still remaining issues. Previous
25 study shows that the OMI NO_2 tropospheric vertical columns processed by the Royal Netherlands Meteorological Institute (KNMI) (DOMINO version 2.0) (Boersma et al., 2011) only underestimated the tropospheric NO_2 VCDs by $\sim$20 % compared to ground based MAX-DOAS observations in Wuxi (another city in Yangtze River Delta) (Wang et al., 2017). In order to investigate the differences between different OMI NO_2 products, we have also plotted the KNMI OMI NO_2 product in Figure 4. The average NO_2 column reported from the KMI product is 10.10×10^{15} molec/cm^2, which is about a factor of 2 higher
30 than the NASA product. The result shows the KNMI product only underestimate the NO_2 columns in Nanjing by $\sim$30 % which is consistent with previous study in Yangtze River Delta (Wang et al., 2017). The difference between the two OMI products can be related to different spectral analysis techniques, stratospheric tropospheric separation algorithms as well as a priori profiles used in the retrievals. Investigation of the differences between the two algorithms is however beyond the scope of this study. Another source of discrepancy is related to the difference in spatial coverage of OMI and MAX-DOAS observations.
35 The spatial coverage of the OMI measurement footprint is ranging from 330 km^2 up to 4600 km^2 with an average of 920 km^2.

Measurements with such large spatial coverage are probably difficult to capture the spatial gradient of NO_2 and resulted in an underestimation over pollution hot spots due to the averaging of large OMI footprint. This effect is especially significant over Nanjing, as it is a local pollution hot spot surrounded by rather clean areas. The underestimation of NO_2 columns is coherent with previous measurements over urban pollution hot spots, i.e., Washington DC and Shanghai (Wenig et al., 2008; Chan et al., 2015). In addition, previous measurements over suburban area in Shanghai show better agreement with OMI observations compared to the measurements in the city (Chan et al., 2015) indicating the effect of spatial inhomogeneity of NO_2 on the satellite data comparison. However, the impact of this effect is difficult to quantify due to lack of high spatial resolution data. Cloud contamination could be an important source of error in the satellite retrieval. Previous study show that the cloud effect on OMI NO_2 VCD retrieval is only significant for cloud radiance fraction > 0.4 (Wang et al., 2017). ~~However,~~ The OMI NO_2 data used in this study are filtered for cloud radiance fraction smaller than 0.4. Therefore, cloud contamination should only show a ~~tiny impact~~ negligible effect in the comparison.

We have also compared the MAX-DOAS and OMI observations of HCHO and both datasets show a similar seasonal variation pattern. The seasonal variation pattern of HCHO is opposite to NO_2 with higher HCHO columns during summer and lower in winter. Higher HCHO levels in summer are ~~mainly~~ related to the increases of biogenic emission of precursor VOCs from plants and higher oxidation rate of VOCs. The MAX-DOAS measurements of HCHO VCDs agree well with the OMI observations with Pearson correlation coefficient (~~R~~R) of 0.75. In addition, the absolute value of the columns show a perfect agreement. The average HCHO VCD measured by the MAX-DOAS is 8.04×10^{15} molec/cm^2 while the averaged OMI HCHO VCD is 7.89×10^{15} molec/cm^2. The slope of the total least squares regression between the two datasets is 0.99 with an offset of 0.31×10^{15} molec/cm^2 (see Figure 4b). ~~Slightly lower HCHO VCDs measured by the~~ In order to quantified the influence of HCHO vertical distribution profile on the air mass factor calculation, we have recomputed the OMI HCHO VCDs using the MAX-DOAS ~~is due~~ HCHO profiles as a priori information. OMI HCHO VCDs retrieved with MAX-DOAS HCHO profiles are also indicated in Figure 4. Using the MAX-DOAS profile as a priori information in the OMI HCHO VCDs retrieval on average increased the OMI HCHO VCDs by $\sim25\%$ with correlation nearly unchanged. The averaged OMI HCHO column over Nanjing increased to 9.95×10^{15} molec/cm^2. The slope of the regression line also increases from 0.99 to 1.39 while the offset reduces from 0.31 to -0.72×10^{15} molec/cm^2. Higher HCHO VCDs retrieved from OMI using MAX-DOAS profiles as a priori is mainly due to the MAX-DOAS measurements are not sensitive to HCHO at higher ~~altitude~~ altitudes. Sources of HCHO in the troposphere include the oxidation of varies of VOCs, including methane. Some of these VOCs have relatively long atmospheric lifetime, e.g., methane, therefore, they are rather well mixed in the atmospheric and resulting in a larger portion of HCHO in the upper troposphere. The MAX-DOAS could not capture HCHO at higher altitudes ~~and results in underestimating~~. Therefore, using the MAX-DOAS profiles for OMI HCHO retrieval is likely underestimated the air mass factors and overestimated the HCHO total columns.

3.3 Seasonal variation of aerosol, NO_2 and HCHO vertical profiles

The seasonal variations of pollutant are closely related to meteorological conditions as well as the characteristics of different emission sources. Analyzing the seasonal variation patterns of different atmospheric pollutants can provide further information
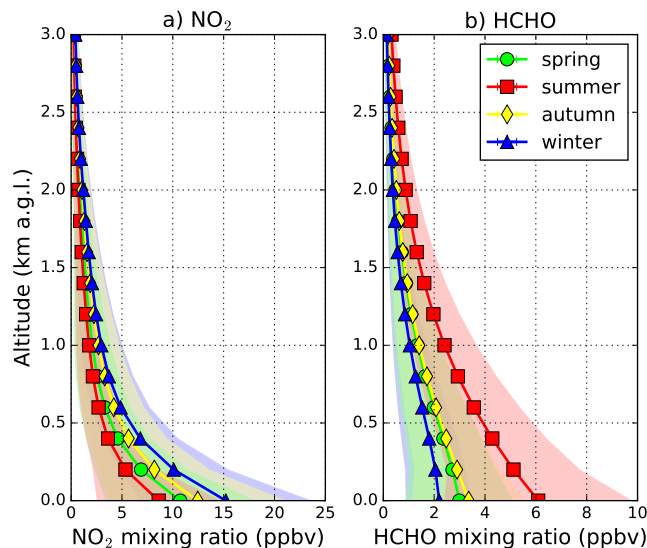
Figure 6. Vertical distribution of (a) aerosol, (b) NO$_2$ and (c) HCHO for different seasons. Shaded areas represent 1 σ standard deviation of variation.

on the emission source characteristic as well as the atmospheric processes. Figure 6 shows the vertical profiles of NO$_2$ and HCHO for all four seasons. Significant seasonal patterns are observed from the NO$_2$ and HCHO data. The NO$_2$ vertical profiles show higher NO$_2$ maxing ratios in autumn and winter and lower in spring and summer. NO$_2$ profiles from all seasons show that the NO$_2$ mixing ratios decrease with increasing altitude. The result indicates most of the measured NO$_2$ is produced close to

5   the surface which agrees with the fact that traffic emission is one of the largest source of atmospheric NO$_2$ in Nanjing. HCHO measurements show a different seasonal variation pattern with lower values during winter and higher mixing ratios in summer. The seasonal pattern of HCHO indicates the significant contribution from biogenic emissions from vegetation. Although HCHO profiles for all seasons also show decreasing mixing ratio with height, the decreasing rate is in general much lower than that of NO$_2$. Larger fraction of HCHO is located at higher altitudes. This is probably related to the source characteristic of HCHO.

10 Majority of the tropospheric HCHO is secondary produced from the oxidation of VOCs and resulting in a larger portion of HCHO in the upper altitudes.

3.4   Regional pollution transport

Air pollutants released to the atmosphere do not only cause local impacts, but also can influence regions far from the source through regional transport. In order to investigate the influences from regional transportation of air pollutants, we use the back-

15 ward trajectories calculated by the HYSPLIT model to back correlate the possible source regions of the MAX-DOAS measured NO$_2$. Similar approaches have also been applied for other source appointment studies (Stohl et al., 2009, 2011; Brunner et al., 2012, 2017; \
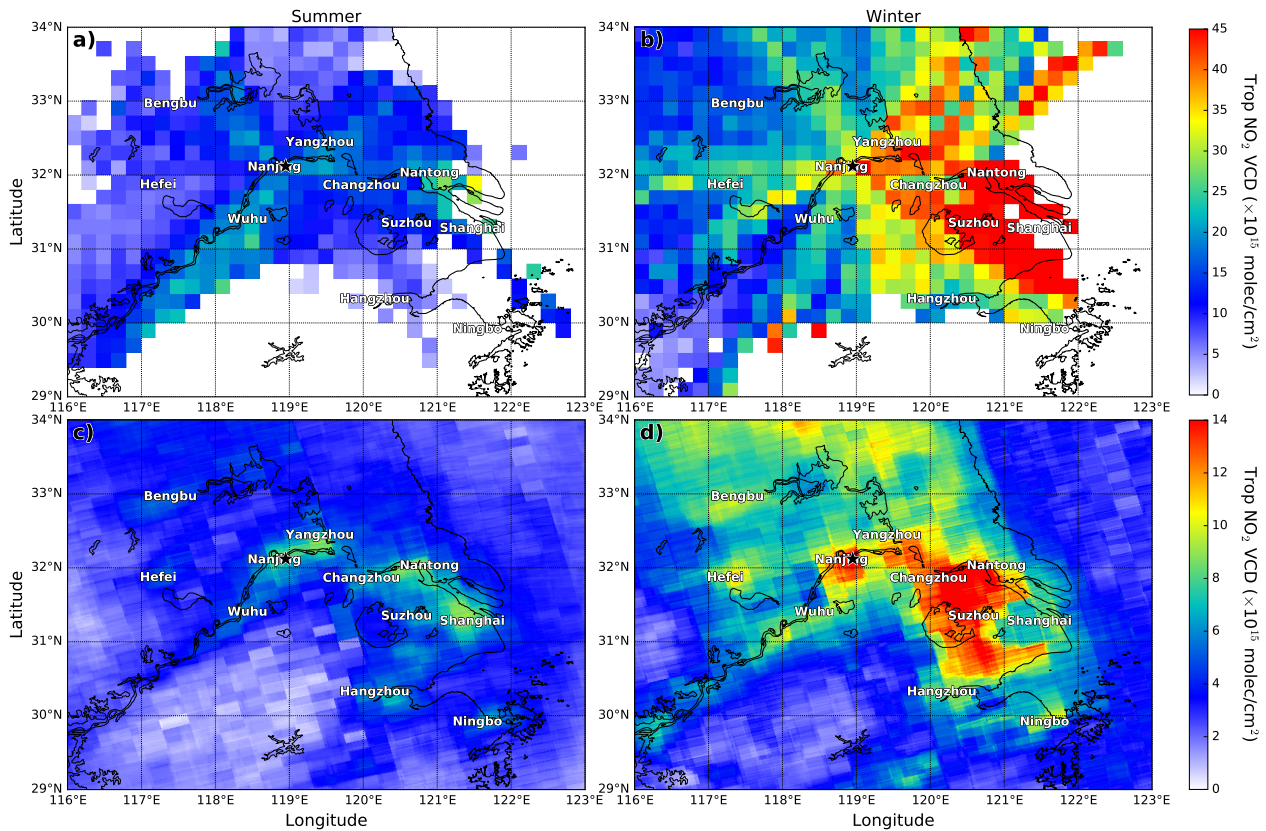
Figure 7. The upper panels show spatial distribution of NO$_2$ in (a) summer and (b) winter reconstructed from the MAX-DOAS measurements using backward trajectories calculated by the HYSPLIT model. Backward trajectories are calculated over 6 h for summer measurements and 12 h for winter measurements. The lower panels indicates the average OMI NO$_2$ vertical column densities over the Yangtze River Delta during (c) summer and (d) winter.

Backward trajectories are calculated at the ~~middle~~ center point of each MAX-DOAS retrieval layer below 2 km. The MAX-DOAS measurement of NO$_2$ partial columns are then assigned to the grid points along the backward trajectories. We assume the partial columns represent a 200 m thick layer of the assigned grid point and the vertical distribution of NO$_2$ in the assigned grid point is assumed to be homogeneous from the surface to 2 km above ground. In this study, the backward propagated NO$_2$

5   data are binned in a resolution of ~~0.25~~0.2° × ~~0.25~~0.2° grid. As NO$_2$ is a relatively short life pollutants in the atmosphere, it is less likely to ~~travel a long distance~~ stay in the atmospheric for a long time and being transported far from the sources. ~~For this reason~~Data are more reliable with shorter atmospheric lifetime. In order to account for this effect, an age weighting factor (w_τ) is used in the backward propagation. The ~~lifetime~~age weighting factor is defined by Eq. 1 where τ is the assumed lifetime of

16
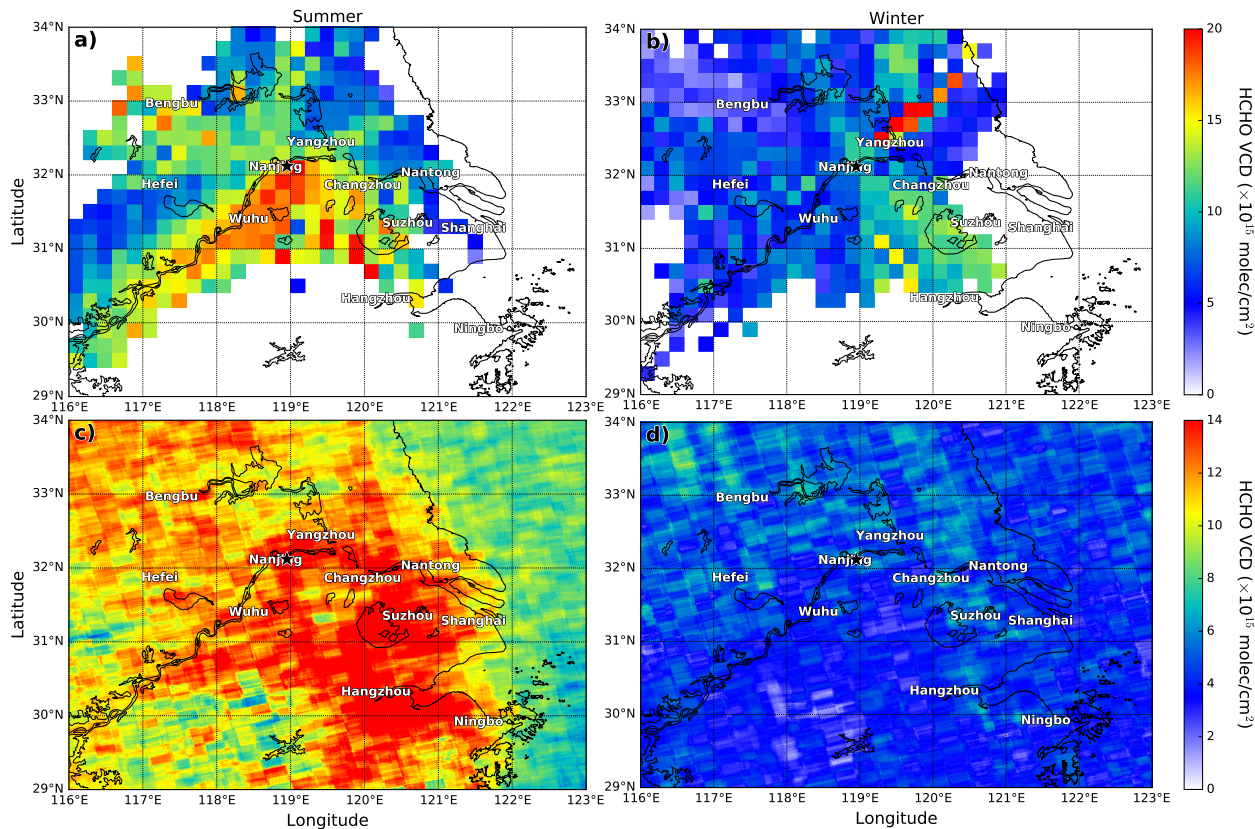
Figure 8. The upper panels show spatial distribution of HCHO in (a) summer and (b) winter reconstructed from the MAX-DOAS measurements using backward trajectories calculated by the HYSPLIT model. Backward trajectories are calculated over 6 h for summer measurements and 12 h for winter measurements. The lower panels indicates the average OMI HCHO vertical column densities over the Yangtze River Delta during (c) summer and (d) winter.

NO_2 and t represents the time for the air mass to travel to the measurement site. This weighting scheme is useful when multiple trajectories overlapping with each other within a single grid point.

$$w_\tau = e^{-\frac{t}{\tau}} \tag{1}$$

As the lifetime of NO_2 has a strong seasonal variability, we separate the measurements into summer (June, July and August) and winter (December, January and February) in our analysis. We assume the NO_2 lifetime in summer and winter is 3 h and 6 h, respectively. Backward trajectories are calculated over 6 h for summer measurements and 12 h for winter measurements. As the assumed lifetime is only used for the calculation of the age factor, the accuracy of the lifetime does not show a strong impact on the reconstructed spatial pattern. In order to get a balance between having better spatial coverage and the reliability

of the reconstructed pollution maps, these numbers are used in this study. NO$_2$ fields reconstructed from the MAX-DOAS measurements in summer and winter using backward trajectories calculated by the HYSPLIT model are shown in Figure 7~~.~~ a&b. Figure 7c&d shows the averaged OMI satellite observations of NO$_2$ ~~and HCHO~~ during summer (June, July and August) and winter (December, January and February) from June 2013 to February 2017. The OMI measurements show that Nanjing

5 has serious NO$_2$ pollution problem in winter~~while HCHO being another air pollution problem during summer~~.

The reconstructed NO$_2$ fields show a good spatial agreement with OMI satellite observations. However, the reconstructed NO$_2$ fields are on average 3 times higher than the OMI observations. ~~This agree well with the fact that~~ As the MAX-DOAS NO$_2$ VCDs are on average 3 times higher than the OMI data, the large discrepancies of the absolute values between the reconstructed data and OMI observations are expected. Elevated NO$_2$ levels are observed during winter when air mass coming

10 from the east, e.g., Shanghai, Suzhou and Nantong, where OMI observations also show high NO$_2$ levels. The summer time NO$_2$ levels are in general lower. However, elevated values can still be observed along the Yangtze River and over some cities, e.g., Nantong and Wuhu.

We have also applied the same approach to the MAX-DOAS HCHO measurements with HCHO lifetime of 1 h and 2 h for summer and winter measurements, respectively. HCHO fields reconstructed from the MAX-DOAS measurements are shown

15 in Figure 8a&b. OMI observations of HCHO are also shown in Figure 8c&d for reference. Summer time HCHO data are in general higher than the observations during winter. However, the spatial distribution of the back propagated HCHO data does not show a strong correlation with the OMI satellite observations as the NO$_2$ data. This is probably due to HCHO is mostly secondary produced in the atmosphere~~and less related to direct emissions~~. In addition, the atmospheric lifetime of HCHO is much shorter compared to NO$_2$ and therefore more dependent on the local productions. The result suggests that the

20 MAX-DOAS measurements are sensitive to the regional transport of air pollutants~~and implied that~~. Despite the strong local contributions, the air quality of Nanjing ~~is~~ can also be significantly influenced by the air pollution transportation, especially during winter.

3.5 Assessments of emission reduction during Youth Olympic

The summer Youth Olympic Games was held from 16 to 28 August 2014 in Nanjing, China. During the event, the govern-

25 ment implemented a series of air pollution control measures. Heavy emission vehicles were strictly prohibited. Local heavy industries, e.g., petrochemical and steel industries were required to limit their production during the Youth Olympic Games. These air pollution control measures were often implemented when such an international events held in China (Wu et al., 2013; Wang et al., 2014; Chan et al., 2015; Liu et al., 2016; Sun et al., 2016). In order to study the influences of the emission control measures implemented during the Youth Olympic Games on the local air quality, we compare the MAX-DOAS observations

30 of aerosol, NO$_2$ and HCHO taken before, during and after the Youth Olympic Games. We define the pre-Olympic period from a month before the Youth Olympic Games (16 July 2014) to 1 day before the Youth Olympic Games (15 August 2014). During the pre-Olympic period, the government gradually started to implement some of the emission control measures. During the Youth Olympic Games all those air pollution control measures were strictly implemented. The post-Olympic period is defined from 29 August 2014 to 28 September 2014 where the emission control was gradually getting back to normal.
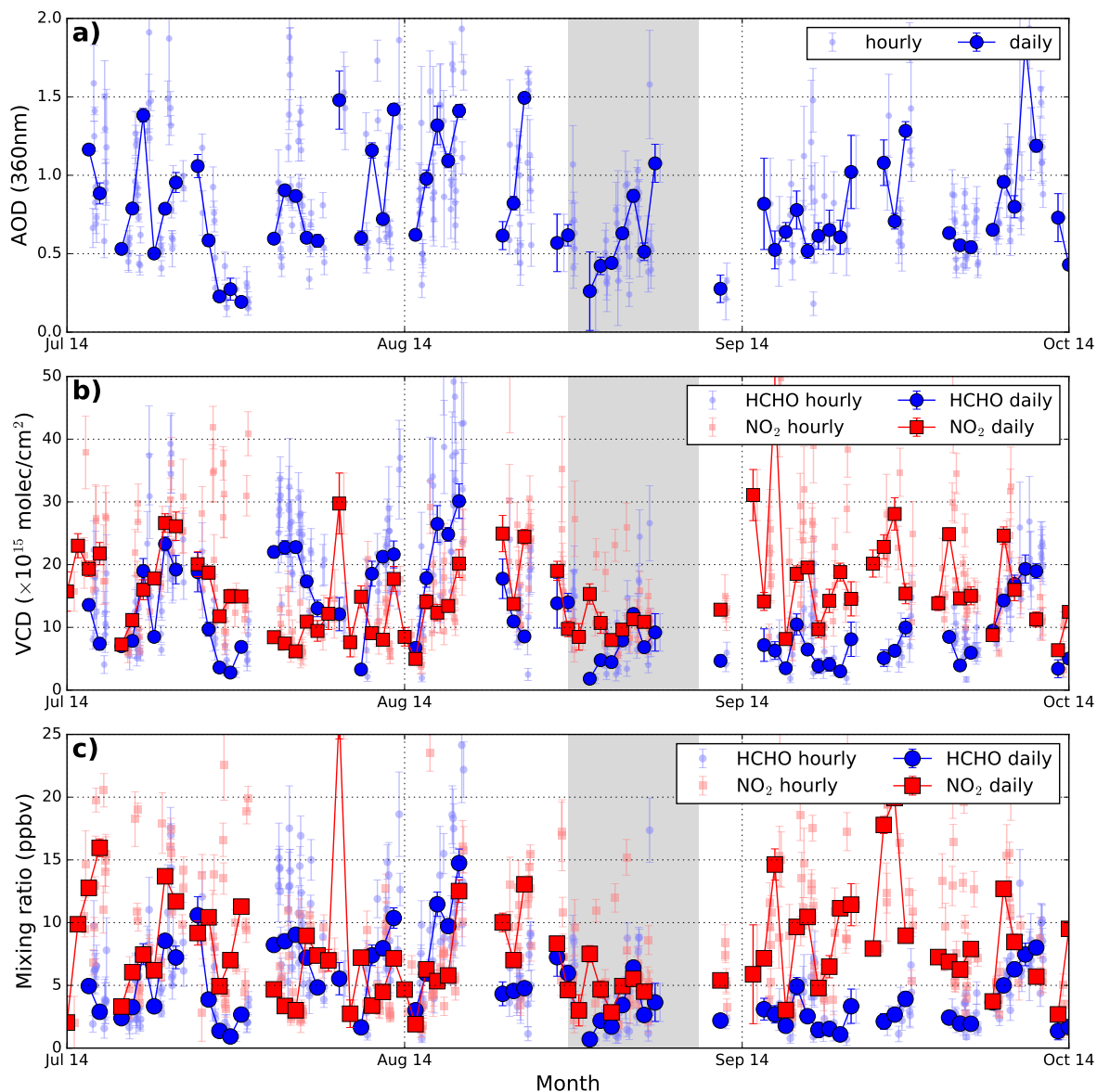
Figure 9. Time series of (a) aerosol optical depths, (b) HCHO and NO_2 VCDs and (c) HCHO and NO_2 surface mixing ratios measured by the MAX-DOAS around the Youth Olympic Games. Hourly and daily averaged values are shown. The gray shadowed area indicates the Youth Olympic Games period (16 to 28 August 2014).

Time series of aerosol optical depths, HCHO and NO_2 VCDs and surface mixing ratios measured by the MAX-DOAS around the Youth Olympic Games are shown in Figure 9. The gray shadowed area indicates the Youth Olympic Games period
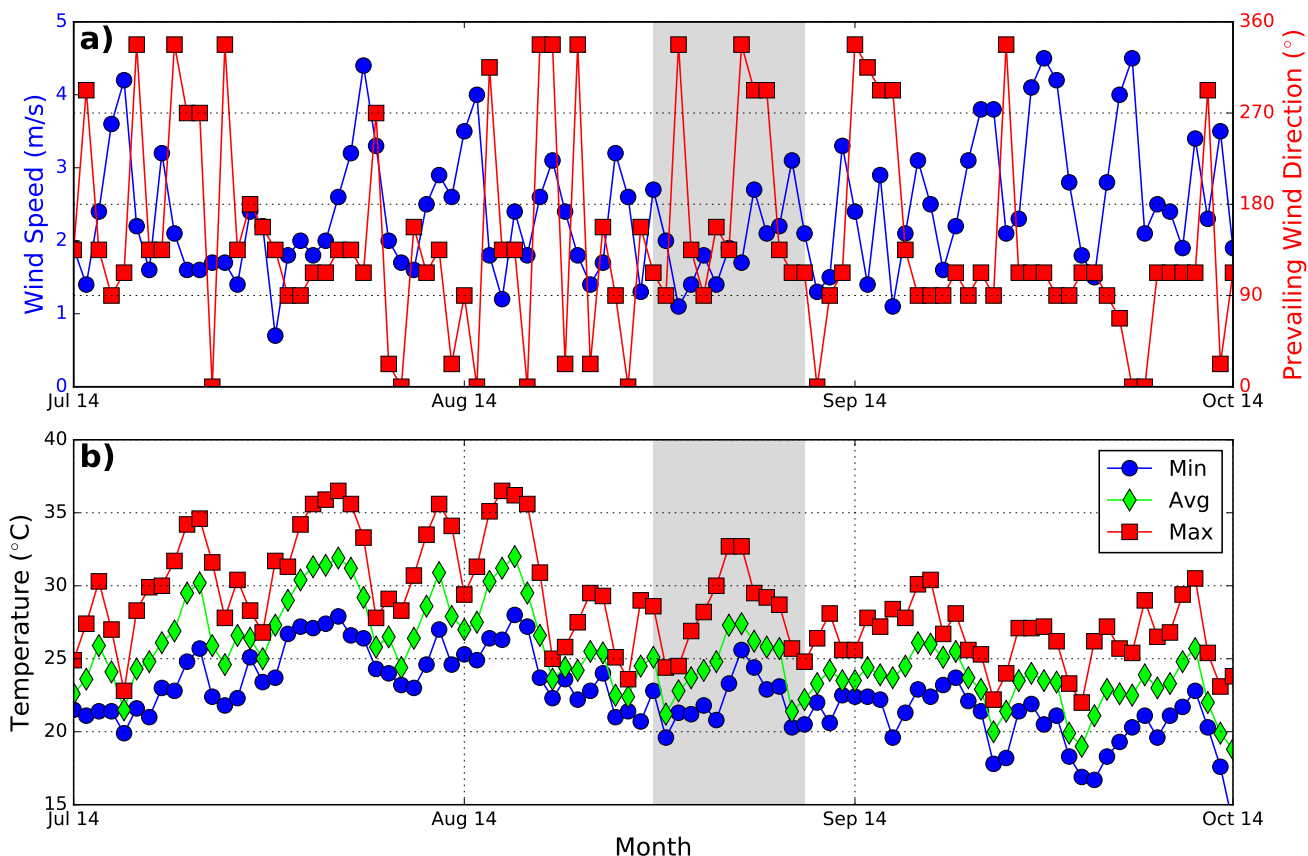
Figure 10. (a) Time series of wind speed (blue curve) and wind direction (red curve). (b) Time series of daily minimum (blue curve), daily average (green curve) and daily maximum temperature. The gray shadowed area indicates the Youth Olympic Games period (16 to 28 August 2014).

(16 to 28 August 2014). Meteorological parameters such as temperature, wind speed and wind direction measured by a weather station in Nanjing during the same period are shown in Figure 10. The AODs, HCHO and NO_2 measurements show a strong temporal variability. In order to investigate the effect of the Youth Olympic Games, we analyzed the statistic of AODs, HCHO and NO_2 VCDs for the pre-Olympic, Olympic and post-Olympic periods. Boxplots of the AODs, HCHO and NO_2 VCDs for the three periods are shown in Figure 11. The results show that AOD, NO_2 and HCHO VCD are the lowest during the Olympic period among those 3 periods. The MAX-DOAS measurements of AOD reduced from 0.9 during the pre-Olympic period to 0.6 for the Olympic period and bounced back to about 0.8 after the Youth Olympic Games. A reduction of NO_2 columns can also be observed during the Youth Olympic Games. Averaged NO_2 VCDs are 14, 11 and 19×10^{15} molec/cm^2 for periods before, during and after the Youth Olympic Games, respectively. Similar reduction pattern is also observed from

20
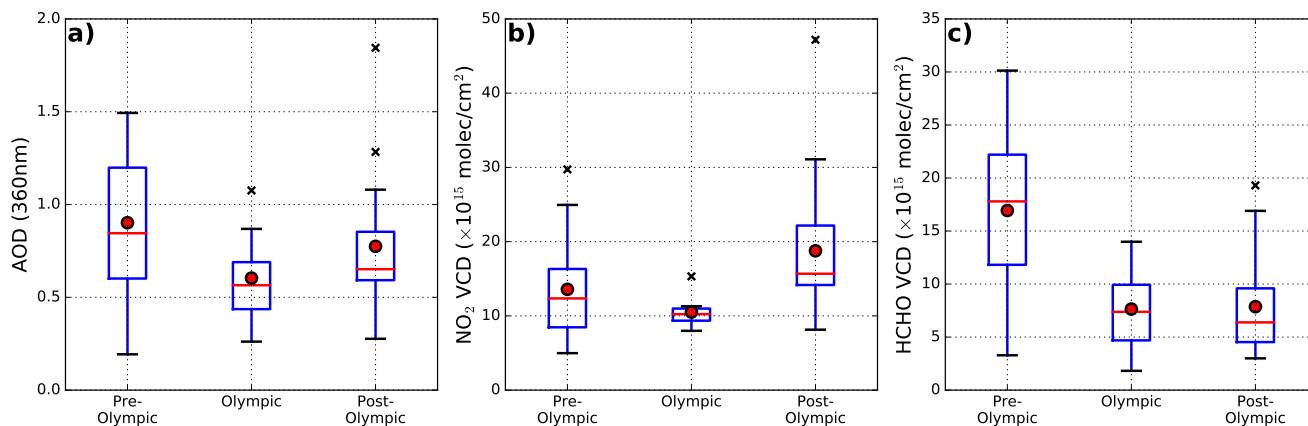
Figure 11. Boxplots of (a) aerosol optical depths, (b) NO$_2$ and (c) HCHO VCDs before, during and after the Youth Olympic Games.

the NO$_2$ surface mixing ratios. Averaged NO$_2$ surface mixing ratios are 7.5, 4.7 and 9.0 ppbv for periods before, during and after the Youth Olympic Games, respectively. The HCHO columns measured during the Youth Olympic Games also decreased by more than ∼50 % from 17×10^{15} molec/cm^2 before the Olympic down to 8×10^{15} molec/cm^2 during the Youth Olympic Games. Surface HCHO mixing ratios also show similar reduction. The surface HCHO mixing ratios measured also reduced
5 from 7.0 ppbv before the Youth Olympic to 3.3 ppbv during the Youth Olympic. As the meteorological conditions are very similar during the three periods, the decrease of pollutant concentrations are mainly attributed to the reduction of emissions during the Youth Olympic Games.

4   Summary and conclusions

In this paper, we present long term observations of atmospheric NO$_2$ and HCHO in Nanjing using a MAX-DOAS instrument.
10 Ground based MAX-DOAS measurements were performed from April 2013 to February 2017. Differential slant columns of O$_4$, NO$_2$ and HCHO were retrieved by applying the differential optical absorption technique to the scattered sun light spectra at the UV band. The results are served as inputs for the retrieval of aerosol extinction, NO$_2$ and HCHO profiles in the lower troposphere.

   Aerosol results derived from the MAX-DOAS observations are validated by comparing the AODs to sun photometer obser-
15 vations. The MAX-DOAS and sun photometer measurements show a good agreement with each other with Pearson correlation coefficient (R) of 0.73. Considering the differences in measurement technique and measurement location, we concluded that the MAX-DOAS aerosol measurements are reliable for the NO$_2$ and HCHO profile retrieval.

   Tropospheric vertical column densities (VCDs) of NO$_2$ derived from MAX-DOAS measurements are used to validate OMI observations. The comparison shows that the OMI observations correlate well with the MAX-DOAS data with Pearson cor-
20 relation coefficient (RR) of 0.91. However, OMI observations are on average ~~a factor of 3~~ 60 % lower than the MAX-DOAS

21

measurements. Using the MAX-DOAS NO$_2$ profile as a priori information in the OMI retrieval on average increased the OMI NO$_2$ VCDs by ~30 % with correlation nearly unchanged. However, the improved OMI NO$_2$ VCDs are still about ~~a factor of 2~~ 50 % lower than the MAX-DOAS observations. The ~~remaining discrepancy is mainly~~ KNMI OMI NO$_2$ product shows a better agreement with the MAX-DOAS observations with an underestimation of ~30 %. Large difference between the two OMI product is related to the different spectral analysis techniques, stratospheric tropospheric separation algorithms as well as a priori profiles used in the retrievals. Another source of discrepancy between MAX-DOAS and OMI observations is related to the difference in spatial coverage between the two measurements. We also compared the OMI observation of HCHO VCDs to our MAX-DOAS data. The result shows a good agreement between the two datasets with ~~R~~ R of 0.75 and the slope of the regression line is 0.99.

The MAX-DOAS measurement of NO$_2$ and HCHO profiles are analyzed together with the backward trajectory simulations to assess the regional transportation and possible source regions of the MAX-DOAS measured NO$_2$ and HCHO. The age weighted backward propagation approach is used to reconstruct the spatial distribution of NO$_2$ and HCHO over the Yangtze River Delta during summer and winter time. The reconstructed NO$_2$ fields show a distinct agreement with OMI satellite observations. The result shows the MAX-DOAS measurements are sensitive to the air pollution transportation in the Yangtze River Delta. However, due to the short atmospheric lifetime of HCHO, the backward propagated HCHO data does not show a strong spatial correlation with the OMI HCHO observations. Our result suggested the air quality of Nanjing are significantly influenced by air pollution transportation, especially during winter.

We have also used the MAX-DOAS observations of aerosol, NO$_2$ and HCHO for the investigation of the effectiveness of air pollution control measures implemented during the Youth Olympic Games 2014. Our results show a significant reduction (30 % - 50 %) of ambient aerosol, NO$_2$ and HCHO compared to measurements before and after the Youth Olympic games. The results indicate the effects of the reduction of emissions during the Youth Olympic Games. Our findings provide a better understanding of the transportation and sources of pollutants in the Yangtze River Delta as well as the effects of emission control measures during large international event, which are important for the future design of air pollution control policies.

22

References

Aliwell, S. R., Roozendael, M. V., Johnston, P. V., Richter, A., Wagner, T., Arlander, D. W., Burrows, J. P., Fish, D. J., Jones, R. L., Tørnkvist, K. K., Lambert, J.-C., Pfeilsticker, K., and Pundt, I.: Analysis for BrO in zenith-sky spectra: An intercomparison exercise for analysis improvement, Journal of Geophysical Research: Atmospheres, 107, ACH 10–1–ACH 10–20, https://doi.org/10.1029/2001JD000329, 2002.

Ångström, A.: On the Atmospheric Transmission of Sun Radiation and on Dust in the Air, Geografiska Annaler, 11, 156–166, https://doi.org/10.1080/20014422.1929.11880498, 1929.

Beirle, S., Platt, U., Wenig, M., and Wagner, T.: Weekly cycle of NO_2 by GOME measurements: a signature of anthropogenic sources, Atmospheric Chemistry and Physics, 3, 2225–2232, https://doi.org/10.5194/acp-3-2225-2003, 2003.

Beirle, S., Platt, U., Wenig, M., and Wagner, T.: NO_x production by lightning estimated with GOME, Advances in Space Research, 34, 793–797, https://doi.org/http://dx.doi.org/10.1016/j.asr.2003.07.069, 2004.

Boersma, K. F., Eskes, H. J., Dirksen, R. J., van der A, R. J., Veefkind, J. P., Stammes, P., Huijnen, V., Kleipool, Q. L., Sneep, M., Claas, J., Leitão, J., Richter, A., Zhou, Y., and Brunner, D.: An improved tropospheric NO_2 column retrieval algorithm for the Ozone Monitoring Instrument, Atmospheric Measurement Techniques, 4, 1905–1928, https://doi.org/10.5194/amt-4-1905-2011, 2011.

Bond, D. W., Zhang, R., Tie, X., Brasseur, G., Huffines, G., Orville, R. E., and Boccippio, D. J.: NO_x production by lightning over the continental United States, Journal of Geophysical Research: Atmospheres, 106, 27 701–27 710, https://doi.org/10.1029/2000JD000191, http://dx.doi.org/10.1029/2000JD000191, 2001.

Bovensmann, H., Burrows, J., Buchwitz, M., Frerick, J., Noël, S., Rozanov, V., Chance, K., and Goede, A.: SCIAMACHY: Mission objectives and measurement modes, Journal of the Atmospheric Sciences, 56, 127–150, 1999.

Brunner, D., Henne, S., Keller, C. A., Reimann, S., Vollmer, M. K., O'Doherty, S., and Maione, M.: An extended Kalman-filter for regional scale inverse emission estimation, Atmospheric Chemistry and Physics, 12, 3455–3478, https://doi.org/10.5194/acp-12-3455-2012, 2012.

Brunner, D., Arnold, T., Henne, S., Manning, A., Thompson, R. L., Maione, M., O'Doherty, S., and Reimann, S.: Comparison of four inverse modelling systems applied to the estimation of HFC-125, HFC-134a, and SF_6 emissions over Europe, Atmospheric Chemistry and Physics, 17, 10 651–10 674, https://doi.org/10.5194/acp-17-10651-2017, 2017.

Bucsela, E. J., Krotkov, N. A., Celarier, E. A., Lamsal, L. N., Swartz, W. H., Bhartia, P. K., Boersma, K. F., Veefkind, J. P., Gleason, J. F., and Pickering, K. E.: A new stratospheric and tropospheric NO_2 retrieval algorithm for nadir-viewing satellite instruments: applications to OMI, Atmospheric Measurement Techniques, 6, 2607–2626, https://doi.org/10.5194/amt-6-2607-2013, 2013.

Burrows, J. P., Weber, M., Buchwitz, M., Rozanov, V., Ladstätter-Weißenmayer, A., Richter, A., DeBeek, R., Hoogen, R., Bramstedt, K., Eichmann, K.-U., et al.: The global ozone monitoring experiment (GOME): Mission concept and first scientific results, Journal of the Atmospheric Sciences, 56, 151–175, 1999.

Callies, J., Corpaccioli, E., Eisinger, M., Hahne, A., and Lefebvre, A.: GOME-2-Metop's second-generation sensor for operational ozone monitoring, ESA bulletin, 102, 28–36, 2000.

Chan, K. L., Pöhler, D., Kuhlmann, G., Hartl, A., Platt, U., and Wenig, M. O.: NO_2 measurements in Hong Kong using LED based long path differential optical absorption spectroscopy, Atmospheric Measurement Techniques, 5, 901–912, https://doi.org/10.5194/amt-5-901-2012, 2012.

Chan, K. L., Hartl, A., Lam, Y. F., Xie, P. H., Liu, W. Q., Cheung, H. M., Lampel, J., Pöhler, D., Li, A., Xu, J., Zhou, H. J., Ning, Z., and Wenig, M.: Observations of tropospheric NO_2 using ground based MAX-DOAS and OMI measurements during the Shanghai World Expo 2010, Atmospheric Environment, 119, 45–58, https://doi.org/http://dx.doi.org/10.1016/j.atmosenv.2015.08.041, 2015.

Chan, K. L., Wiegner, M., Wenig, M., and Pöhler, D.: Observations of tropospheric aerosols and NO_2 in Hong Kong over 5 years using ground based MAX-DOAS, Science of The Total Environment, 619-620, 1545 – 1556, https://doi.org/https://doi.org/10.1016/j.scitotenv.2017.10.153, 2018.

Clémer, K., Van Roozendael, M., Fayt, C., Hendrick, F., Hermans, C., Pinardi, G., Spurr, R., Wang, P., and De Mazière, M.: Multiple wavelength retrieval of tropospheric aerosol optical properties from MAXDOAS measurements in Beijing, Atmospheric Measurement Techniques, 3, 863–878, https://doi.org/10.5194/amt-3-863-2010, 2010.

Cleveland, W. S.: LOWESS: A Program for Smoothing Scatterplots by Robust Locally Weighted Regression, The American Statistician, 35, https://doi.org/10.2307/2683591, 1981.

Crutzen, P. J.: The influence of nitrogen oxides on the atmospheric ozone content, Quarterly Journal of the Royal Meteorological Society, 96, 320–325, https://doi.org/10.1002/qj.49709640815, 1970.

De Smedt, I., Theys, N., Yu, H., Danckaert, T., Lerot, C., Compernolle, S., Van Roozendael, M., Richter, A., Hilboll, A., Peters, E., Pedergnana, M., Loyola, D., Beirle, S., Wagner, T., Eskes, H., van Geffen, J., Boersma, K. F., and Veefkind, P.: Algorithm theoretical baseline for formaldehyde retrievals from S5P TROPOMI and from the QA4ECV project, Atmospheric Measurement Techniques, 11, 2395–2426, https://doi.org/10.5194/amt-11-2395-2018, 2018.

Emde, C., Buras-Schnell, R., Kylling, A., Mayer, B., Gasteiger, J., Hamann, U., Kylling, J., Richter, B., Pause, C., Dowling, T., and Bugliaro, L.: The libRadtran software package for radiative transfer calculations (version 2.0.1), Geoscientific Model Development, 9, 1647–1672, https://doi.org/10.5194/gmd-9-1647-2016, 2016.

Fleischmann, O. C., Burrows, J. P., and Orphal, J.: Time-windowing Fourier transform absorption spectroscopy for flash photolysis investigations, Journal of Photochemistry and Photobiology A: Chemistry, 157, 127–136, https://doi.org/http://dx.doi.org/10.1016/S1010-6030(03)00069-8, atmospheric Photochemistry, 2003.

Fried, A., Cantrell, C., Olson, J., Crawford, J. H., Weibring, P., Walega, J., Richter, D., Junkermann, W., Volkamer, R., Sinreich, R., Heikes, B. G., O'Sullivan, D., Blake, D. R., Blake, N., Meinardi, S., Apel, E., Weinheimer, A., Knapp, D., Perring, A., Cohen, R. C., Fuelberg, H., Shetter, R. E., Hall, S. R., Ullmann, K., Brune, W. H., Mao, J., Ren, X., Huey, L. G., Singh, H. B., Hair, J. W., Riemer, D., Diskin, G., and Sachse, G.: Detailed comparisons of airborne formaldehyde measurements with box models during the 2006 INTEX-B and MILAGRO campaigns: potential evidence for significant impacts of unmeasured and multi-generation volatile organic carbon compounds, Atmospheric Chemistry and Physics, 11, 11 867–11 894, https://doi.org/10.5194/acp-11-11867-2011, 2011.

Frieß, U., Monks, P. S., Remedios, J. J., Rozanov, A., Sinreich, R., Wagner, T., and Platt, U.: MAX-DOAS O_4 measurements: A new technique to derive information on atmospheric aerosols: 2. Modeling studies, Journal of Geophysical Research: Atmospheres, 111, https://doi.org/10.1029/2005JD006618, 2006.

González Abad, G., Liu, X., Chance, K., Wang, H., Kurosu, T. P., and Suleiman, R.: Updated Smithsonian Astrophysical Observatory Ozone Monitoring Instrument (SAO OMI) formaldehyde retrieval, Atmospheric Measurement Techniques, 8, 19–32, https://doi.org/10.5194/amt-8-19-2015, 2015.

Halla, J. D., Wagner, T., Beirle, S., Brook, J. R., Hayden, K. L., O'Brien, J. M., Ng, A., Majonis, D., Wenig, M. O., and McLaren, R.: Determination of tropospheric vertical columns of NO_2 and aerosol optical properties in a rural setting using MAX-DOAS, Atmospheric Chemistry and Physics, 11, 12 475–12 498, https://doi.org/10.5194/acp-11-12475-2011, 2011.

Hartl, A. and Wenig, M. O.: Regularisation model study for the least-squares retrieval of aerosol extinction time series from UV/VIS MAX-DOAS observations for a ground layer profile parameterisation, Atmospheric Measurement Techniques, 6, 1959–1980, https://doi.org/10.5194/amt-6-1959-2013, 2013.

Hönninger, G. and Platt, U.: Observations of BrO and its vertical distribution during surface ozone depletion at Alert, Atmospheric Environment, 36, 2481–2489, https://doi.org/http://dx.doi.org/10.1016/S1352-2310(02)00104-8, 2002.

Hönninger, G., von Friedeburg, C., and Platt, U.: Multi axis differential optical absorption spectroscopy (MAX-DOAS), Atmospheric Chemistry and Physics, 4, 231–254, https://doi.org/10.5194/acp-4-231-2004, 2004.

5 Irie, H., Kanaya, Y., Akimoto, H., Iwabuchi, H., Shimizu, A., and Aoki, K.: First retrieval of tropospheric aerosol profiles using MAX-DOAS and comparison with lidar and sky radiometer measurements, Atmospheric Chemistry and Physics, 8, 341–350, https://doi.org/10.5194/acp-8-341-2008, 2008.

Jang, M. and Kamens, R. M.: Characterization of Secondary Aerosol from the Photooxidation of Toluene in the Presence of NO_x and 1-Propene, Environmental Science & Technology, 35, 3626–3639, https://doi.org/10.1021/es010676+, 2001.

10 Jin, J., Ma, J., Lin, W., Zhao, H., Shaiganfar, R., Beirle, S., and Wagner, T.: MAX-DOAS measurements and satellite validation of tropospheric NO_2 and SO_2 vertical column densities at a rural site of North China, Atmospheric Environment, 133, 12–25, https://doi.org/http://dx.doi.org/10.1016/j.atmosenv.2016.03.031, 2016.

Krotkov, N. A., Lamsal, L. N., Celarier, E. A., Swartz, W. H., Marchenko, S. V., Bucsela, E. J., Chan, K. L., Wenig, M., and Zara, M.: The version 3 OMI NO_2 standard product, Atmospheric Measurement Techniques, 10, 3133–3149, https://doi.org/10.5194/amt-10-3133-2017, 15 2017.

Levelt, P., Van den Oord, G. H. J., Dobber, M., Malkki, A., Visser, H., de Vries, J., Stammes, P., Lundell, J., and Saari, H.: The ozone monitoring instrument, Geoscience and Remote Sensing, IEEE Transactions on, 44, 1093–1101, https://doi.org/10.1109/TGRS.2006.872333, 2006.

Li, X., Brauers, T., Shao, M., Garland, R. M., Wagner, T., Deutschmann, T., and Wahner, A.: MAX-DOAS measurements in southern China: 20 retrieval of aerosol extinctions and validation using ground-based in-situ data, Atmospheric Chemistry and Physics, 10, 2079–2089, https://doi.org/10.5194/acp-10-2079-2010, 2010.

Li, X., Brauers, T., Hofzumahaus, A., Lu, K., Li, Y. P., Shao, M., Wagner, T., and Wahner, A.: MAX-DOAS measurements of NO_2, HCHO and CHOCHO at a rural site in Southern China, Atmospheric Chemistry and Physics, 13, 2133–2151, https://doi.org/10.5194/acp-13-2133-2013, 2013.

25 Lin, J.-T., Martin, R. V., Boersma, K. F., Sneep, M., Stammes, P., Spurr, R., Wang, P., Van Roozendael, M., Clémer, K., and Irie, H.: Retrieving tropospheric nitrogen dioxide from the Ozone Monitoring Instrument: effects of aerosols, surface reflectance anisotropy, and vertical profile of nitrogen dioxide, Atmospheric Chemistry and Physics, 14, 1441–1461, https://doi.org/10.5194/acp-14-1441-2014, 2014.

Liu, H., Liu, C., Xie, Z., Li, Y., Huang, X., Wang, S., Xu, J., and Xie, P.: A paradox for air pollution controlling in China revealed by "APEC Blue" and "Parade Blue", Scientific Reports, 6, 34 408, 2016.

30 Ma, J. Z., Beirle, S., Jin, J. L., Shaiganfar, R., Yan, P., and Wagner, T.: Tropospheric NO_2 vertical column densities over Beijing: results of the first three years of ground-based MAX-DOAS measurements (2008-2011) and satellite validation, Atmospheric Chemistry and Physics, 13, 1547–1567, https://doi.org/10.5194/acp-13-1547-2013, 2013.

Marchenko, S., Krotkov, N. A., Lamsal, L. N., Celarier, E. A., Swartz, W. H., and Bucsela, E. J.: Revising the slant column density retrieval of nitrogen dioxide observed by the Ozone Monitoring Instrument, Journal of Geophysical Research: Atmospheres, 120, 5670–5692, 35 https://doi.org/10.1002/2014JD022913, http://dx.doi.org/10.1002/2014JD022913, 2014JD022913, 2015.

Meller, R. and Moortgat, G. K.: Temperature dependence of the absorption cross sections of formaldehyde between 223 and 323 K in the wavelength range 225-375 nm, Journal of Geophysical Research: Atmospheres, 105, 7089–7101, https://doi.org/10.1029/1999JD901074, 2000.

Mijling, B., van der A, R. J., Boersma, K. F., Van Roozendael, M., De Smedt, I., and Kelder, H. M.: Reductions of NO_2 detected from space during the 2008 Beijing Olympic Games, Geophysical Research Letters, 36, https://doi.org/10.1029/2009GL038943, 2009.

Ortega, I., Berg, L. K., Ferrare, R. A., Hair, J. W., Hostetler, C. A., and Volkamer, R.: Elevated aerosol layers modify the O_2-O_2 absorption measured by ground-based MAX-DOAS, Journal of Quantitative Spectroscopy and Radiative Transfer, 176, 34–49, https://doi.org/https://doi.org/10.1016/j.jqsrt.2016.02.021, 2016.

Platt, U. and Stutz, J.: Differential optical absorption spectroscopy - principles and applications, Springer, 2008.

Richter, A., Burrows, J. P., Nüß, H., Granier, C., and Niemeier, U.: Increase in tropospheric nitrogen dioxide over China observed from space, Nature, 437, 129–132, 2005.

Rodgers, C. D.: Inverse methods for atmospheric sounding: Theory and practice, vol. 2, World scientific, 2000.

Rotman, D. A., Tannahill, J. R., Kinnison, D. E., Connell, P. S., Bergmann, D., Proctor, D., Rodriguez, J. M., Lin, S. J., Rood, R. B., Prather, M. J., Rasch, P. J., Considine, D. B., Ramaroson, R., and Kawa, S. R.: Global Modeling Initiative assessment model: Model description, integration, and testing of the transport shell, Journal of Geophysical Research: Atmospheres, 106, 1669–1691, https://doi.org/10.1029/2000JD900463, 2001.

Serdyuchenko, A., Gorshelev, V., Weber, M., Chehade, W., and Burrows, J. P.: High spectral resolution ozone absorption cross-sections - Part 2: Temperature dependence, Atmospheric Measurement Techniques, 7, 625–636, https://doi.org/10.5194/amt-7-625-2014, 2014.

Sinreich, R., Frieß, U., Wagner, T., and Platt, U.: Multi axis differential optical absorption spectroscopy (MAX-DOAS) of gas and aerosol distributions, Faraday Discussions, 130, 153, https://doi.org/10.1039/b419274p, 2005.

Solomon, S., Schmeltekopf, A. L., and Sanders, R. W.: On the interpretation of zenith sky absorption measurements, Journal of Geophysical Research: Atmospheres, 92, 8311–8319, https://doi.org/10.1029/JD092iD07p08311, 1987.

Stein, A. F., Draxler, R. R., Rolph, G. D., Stunder, B. J. B., Cohen, M. D., and Ngan, F.: NOAA's HYSPLIT Atmospheric Transport and Dispersion Modeling System, Bulletin of the American Meteorological Society, 96, 2059–2077, https://doi.org/10.1175/BAMS-D-14-00110.1, 2015.

Stohl, A., Seibert, P., Arduini, J., Eckhardt, S., Fraser, P., Greally, B. R., Lunder, C., Maione, M., Mühle, J., O'Doherty, S., Prinn, R. G., Reimann, S., Saito, T., Schmidbauer, N., Simmonds, P. G., Vollmer, M. K., Weiss, R. F., and Yokouchi, Y.: An analytical inversion method for determining regional and global emissions of greenhouse gases: Sensitivity studies and application to halocarbons, Atmospheric Chemistry and Physics, 9, 1597–1620, https://doi.org/10.5194/acp-9-1597-2009, 2009.

Stohl, A., Prata, A. J., Eckhardt, S., Clarisse, L., Durant, A., Henne, S., Kristiansen, N. I., Minikin, A., Schumann, U., Seibert, P., Stebel, K., Thomas, H. E., Thorsteinsson, T., Tørseth, K., and Weinzierl, B.: Determination of time- and height-resolved volcanic ash emissions and their use for quantitative ash dispersion modeling: the 2010 Eyjafjallajökull eruption, Atmospheric Chemistry and Physics, 11, 4333–4351, https://doi.org/10.5194/acp-11-4333-2011, 2011.

Sun, Y., Wang, Z., Wild, O., Xu, W., Chen, C., Fu, P., Du, W., Zhou, L., Zhang, Q., Han, T., Wang, Q., Pan, X., Zheng, H., Li, J., Guo, X., Liu, J., and Worsnop, D. R.: "APEC Blue": Secondary Aerosol Reductions from Emission Controls in Beijing, Scientific Reports, 6, 20 668, 2016.

Thalman, R. and Volkamer, R.: Temperature dependent absorption cross-sections of O_2-O_2 collision pairs between 340 and 630 nm and at atmospherically relevant pressure, Phys. Chem. Chem. Phys., 15, 15 371–15 381, https://doi.org/10.1039/C3CP50968K, 2013.

van der A, R. J., Eskes, H. J., Boersma, K. F., van Noije, T. P. C., Van Roozendael, M., De Smedt, I., Peters, D. H. M. U., and Meijer, E. W.: Trends, seasonal variability and dominant NO_x source derived from a ten year record of NO_2 measured from space, Journal of Geophysical Research: Atmospheres, 113, https://doi.org/10.1029/2007JD009021, 2008.

Vandaele, A., Hermans, C., Simon, P., Carleer, M., Colin, R., Fally, S., Merienne, M., Jenouvrier, A., and Coquart, B.: Measurements of the NO_2 absorption cross-section from $42000\,cm^{-1}$ to $10000\,cm^{-1}$ (238-1000 nm) at 220 K and 294 K, Journal of Quantitative Spectroscopy and Radiative Transfer, 59, 171 – 184, https://doi.org/http://dx.doi.org/10.1016/S0022-4073(97)00168-4, atmospheric Spectroscopy Applications 96, 1998.

5   Wagner, T., Dix, B., Friedeburg, C. v., Fries, U., Sanghavi, S., Sinreich, R., and Platt, U.: MAX-DOAS O_4 measurements: A new technique to derive information on atmospheric aerosols - Principles and information content, Journal of Geophysical Research: Atmospheres, 109, https://doi.org/10.1029/2004JD004904, 2004.

Wagner, T., Deutschmann, T., and Platt, U.: Determination of aerosol properties from MAX-DOAS observations of the Ring effect, Atmospheric Measurement Techniques, 2, 495–512, https://doi.org/10.5194/amt-2-495-2009, 2009.

10   Wagner, T., Beirle, S., Brauers, T., Deutschmann, T., Frieß, U., Hak, C., Halla, J. D., Heue, K. P., Junkermann, W., Li, X., Platt, U., and Pundt-Gruber, I.: Inversion of tropospheric profiles of aerosol extinction and HCHO and NO_2 mixing ratios from MAX-DOAS observations in Milano during the summer of 2003 and comparison with independent data sets, Atmospheric Measurement Techniques, 4, 2685–2715, https://doi.org/10.5194/amt-4-2685-2011, 2011.

Wagner, T., Beirle, S., Benavent, N., Bösch, T., Chan, K. L., Donner, S., Dörner, S., Fayt, C., Frieß, U., García-Nieto, D., Gielen, C.,
15   González-Bartolome, D., Gomez, L., Hendrick, F., Henzing, B., Jin, J. L., Lampel, J., Ma, J., Mies, K., Navarro, M., Peters, E., Pinardi, G., Puentedura, O., Puķīte, J., Remmers, J., Richter, A., Saiz-Lopez, A., Shaiganfar, R., Sihler, H., Van Roozendael, M., Wang, Y., and Yela, M.: Is a scaling factor required to obtain closure between measured and modelled atmospheric O_4 absorptions? - A case study for two days during the MADCAT campaign, Atmospheric Measurement Techniques Discussions, 2018, 1–85, https://doi.org/10.5194/amt-2018-238, 2018.

20   Wang, S., Gao, J., Zhang, Y., Zhang, J., Cha, F., Wang, T., Ren, C., and Wang, W.: Impact of emission control on regional air quality: An observational study of air pollutants before, during and after the Beijing Olympic Games, Journal of Environmental Sciences, 26, 175 – 180, https://doi.org/https://doi.org/10.1016/S1001-0742(13)60395-2, 2014.

Wang, S., Cuevas, C. A., Frieß, U., and Saiz-Lopez, A.: MAX-DOAS retrieval of aerosol extinction properties in Madrid, Spain, Atmospheric Measurement Techniques, 9, 5089–5101, https://doi.org/10.5194/amt-9-5089-2016, 2016.

25   Wang, Y., Beirle, S., Lampel, J., Koukouli, M., De Smedt, I., Theys, N., Li, A., Wu, D., Xie, P., Liu, C., Van Roozendael, M., Stavrakou, T., Müller, J.-F., and Wagner, T.: Validation of OMI, GOME-2A and GOME-2B tropospheric NO_2, SO_2 and HCHO products using MAX-DOAS observations from 2011 to 2014 in Wuxi, China: investigation of the effects of priori profiles and aerosols on the satellite products, Atmospheric Chemistry and Physics, 17, 5007–5033, https://doi.org/10.5194/acp-17-5007-2017, 2017.

Wang, Y., Dörner, S., Donner, S., Böhnke, S., De Smedt, I., Dickerson, R. R., Dong, Z., He, H., Li, Z., Li, Z., Li, D., Liu, D., Ren, X.,
30   Theys, N., Wang, Y., Wang, Y., Wang, Z., Xu, H., Xu, J., and Wagner, T.: Vertical profiles of NO_2, SO_2, HONO, HCHO, CHOCHO and aerosols derived from MAX-DOAS measurements at a rural site in the central western North China Plain and their relation to emission sources and effects of regional transport, Atmospheric Chemistry and Physics, 19, 5417–5449, https://doi.org/10.5194/acp-19-5417-2019, https://www.atmos-chem-phys.net/19/5417/2019/, 2019.

Wenig, M., Spichtinger, N., Stohl, A., Held, G., Beirle, S., Wagner, T., Jähne, B., and Platt, U.: Intercontinental transport of nitrogen oxide
35   pollution plumes, Atmospheric Chemistry and Physics, 3, 387–393, https://doi.org/10.5194/acp-3-387-2003, 2003.

Wenig, M. O., Cede, A. M., Bucsela, E. J., Celarier, E. A., Boersma, K. F., Veefkind, J. P., Brinksma, E. J., Gleason, J. F., and Herman, J. R.: Validation of OMI tropospheric NO_2 column densities using direct-Sun mode Brewer measurements at NASA Goddard Space Flight Center, Journal of Geophysical Research: Atmospheres, 113, https://doi.org/10.1029/2007JD008988, 2008.

Witte, J. C., Schoeberl, M. R., Douglass, A. R., Gleason, J. F., Krotkov, N. A., Gille, J. C., Pickering, K. E., and Livesey, N.: Satellite observations of changes in air quality during the 2008 Beijing Olympics and Paralympics, Geophysical Research Letters, 36, https://doi.org/10.1029/2009GL039236, 2009.

Wittrock, F., Oetjen, H., Richter, A., Fietkau, S., Medeke, T., Rozanov, A., and Burrows, J. P.: MAX-DOAS measurements of atmospheric trace gases in Ny-Alesund - Radiative transfer studies and their application, Atmospheric Chemistry and Physics, 4, 955–966, https://doi.org/10.5194/acp-4-955-2004, 2004.

Wu, F. C., Xie, P. H., Li, A., Chan, K. L., Hartl, A., Wang, Y., Si, F. Q., Zeng, Y., Qin, M., Xu, J., Liu, J. G., Liu, W. Q., and Wenig, M.: Observations of SO_2 and NO_2 by mobile DOAS in the Guangzhou eastern area during the Asian Games 2010, Atmospheric Measurement Techniques, 6, 2277–2292, https://doi.org/10.5194/amt-6-2277-2013, 2013.

Zhang, J., Wang, S., Guo, Y., Zhang, R., Qin, X., Huang, K., Wang, D., Fu, Q., Wang, J., and Zhou, B.: Aerosol vertical profile retrieved from ground-based MAX-DOAS observation and characteristic distribution during wintertime in Shanghai, China, Atmospheric Environment, 192, 193 – 205, https://doi.org/https://doi.org/10.1016/j.atmosenv.2018.08.051, 2018.

Zhang, Q., Streets, D. G., He, K., Wang, Y., Richter, A., Burrows, J. P., Uno, I., Jang, C. J., Chen, D., Yao, Z., and Lei, Y.: NO_x emission trends for China, 1995-2004: The view from the ground and the view from space, Journal of Geophysical Research: Atmospheres, 112, https://doi.org/10.1029/2007JD008684, 2007.

Zhang, R., Tie, X., and Bond, D. W.: Impacts of anthropogenic and natural NO_x sources over the U.S. on tropospheric chemistry, Proceedings of the National Academy of Sciences, 100, 1505–1509, https://doi.org/10.1073/pnas.252763799, 2003.

Zhao, B., Wang, S. X., Liu, H., Xu, J. Y., Fu, K., Klimont, Z., Hao, J. M., He, K. B., Cofala, J., and Amann, M.: NO_x emissions in China: historical trends and future perspectives, Atmospheric Chemistry and Physics, 13, 9869–9897, https://doi.org/10.5194/acp-13-9869-2013, 2013.